Title

Ablation of Transcription Factor IRF4 Promotes Transplant Acceptance by Driving Allogenic CD4+ T Cell Dysfunction

Journal

Immunity, 47(6)

ISSN

1074-7613

Authors

Wu, Jie
Zhang, Hedong
Shi, Xiaomin
et al.

Publication Date

2017-12-01

DOI

10.1016/j.immuni.2017.11.003

Peer reviewed

HHS Public Access

Author manuscript

Immunity. Author manuscript; available in PMC 2018 December 19.

Published in final edited form as:

Immunity. 2017 December 19; 47(6): 1114–1128.e6. doi:10.1016/j.immuni.2017.11.003.

Ablation of transcription factor IRF4 promotes transplant acceptance by driving allogenic CD4+ T cell dysfunction

Jie Wu[1,2], **Hedong Zhang**[1], **Xiaomin Shi**[1], **Xiang Xiao**[1], **Yihui Fan**[1], **Laurie J. Minze**[1], **Jin Wang**[1,3], **Rafik M. Ghobrial**[1,3], **Jiahong Xia**[2], **Roger Sciammas**[1,4], **Xian C. Li**[1,3], and **Wenhao Chen**[1,3,*]

[1]Immunobiology & Transplant Science Center, Houston Methodist Research Institute, Texas Medical Center, Houston, TX 77030, USA

[2]Department of Cardiovascular Surgery, Union Hospital, Tongji Medical College, Huazhong University of Science and Technology, Wuhan, Hubei 430030, China

[3]Department of Surgery, Weill Cornell Medical College of Cornell University, New York, NY10065, USA

[4]Center for Comparative Medicine, University of California Davis, Davis, CA 95616, USA

SUMMARY

CD4+ T cells orchestrate immune responses and destruction of allogeneic organ transplants, but how this process is regulated on a transcriptional level remains unclear. Here, we demonstrated that interferon regulatory factor 4 (IRF4) was a key transcriptional determinant controlling T cell responses during transplantation. IRF4 deletion in mice resulted in progressive establishment of CD4+ T cell dysfunction and long-term allograft survival. Mechanistically, IRF4 repressed PD-1, Helios, and other molecules associated with T cell dysfunction. In the absence of IRF4, chromatin accessibility and binding of Helios at PD-1 *cis*-regulatory elements were increased, resulting in enhanced PD-1 expression and CD4+ T cell dysfunction. The dysfunctional state of *Irf4*-deficient T cells was initially reversible by PD-1 ligand blockade, but it progressively developed into an irreversible state. Hence, IRF4 controls a core regulatory circuit of CD4+ T cell dysfunction, and targeting IRF4 represents a potential therapeutic strategy for achieving transplant acceptance.

eTOC Blurb

CD4+ T cells drive allogeneic organ transplant destruction, but how this is regulated transcriptionally remains unclear. Wu et al. report that IRF4 deletion in T cells leads to the

*Lead Contact and Correspondence: W.C. (wchen@houstonmethosit.org). Immunobiology & Transplant Science Center, Houston Methodist Research Institute, 6670 Bertner Avenue, R7-216, Houston, TX 77030, USA. Telephone: 713.441.2173, Fax: 713.441.7439.

AUTHOR CONTRIBUTIONS

J.W., R.S., X.X., X.C.L, and W.C. conceived and designed the research. J.W. carried out most of the experiments with help from H.Z, X.S., X.X., and Y.F.; W.C. performed heart transplantations; R.S. established the *Irf4*$^{-/-}$ TEa mouse. J.W., R.S., X.X., L.J.M, R.M.G, J.W., J.X, X.C.L., and W.C. analyzed results and discussed the results; and W.C. and X.C.L coordinated this work and wrote the manuscript.

establishment of T cell dysfunction and long-term allograft survival. Therefore, targeting IRF4 represents a therapeutic opportunity for achieving transplant acceptance.

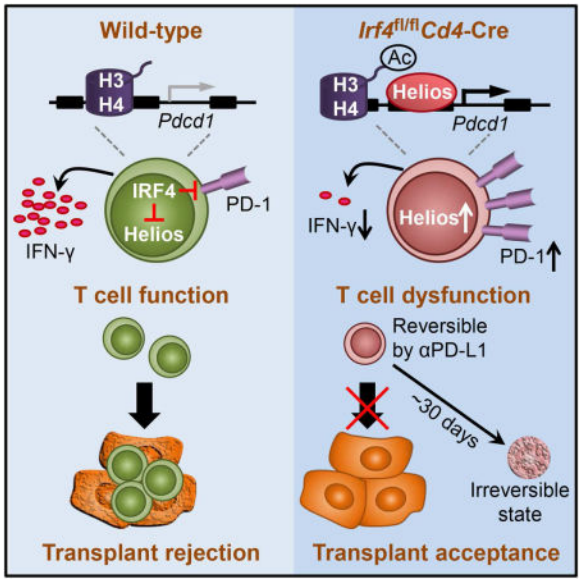

INTRODUCTION

In organ transplantation, $CD4^+$ but not $CD8^+$ T cells are essential for allo-rejection, as it has been shown that $CD4^+$ T cells are necessary and sufficient for mediating acute rejection of heart and kidney allografts (Bolton et al., 1989; Krieger et al. 1996). Among $CD4^+$ T cell subsets, alloreactive T helper 1 (Th1) cells have been shown to cause allograft damage directly through Fas-Fas ligand–mediated cytotoxicity, or indirectly through inducing delayed type hypersensitivity by macrophages and promoting the activity of cytotoxic $CD8^+$ T cells (Liu et al. 2013). Th17 cells also mediate allograft rejection, which has been demonstrated in recipient mice lacking of T-bet, the master regulator of Th1 cell differentiation (Yuan et al., 2008). T follicular helper (Tfh) cells contribute to allograft rejection by promoting alloantibody responses (Conlon et al., 2012). By contrast, $CD4^+Foxp3^+$ regulatory (Treg) cells protect the transplanted organs from rejection in many experimental models (Miyahara et al., 2012; Safinia et al., 2015).

T cell dysfunction, such as exhaustion and anergy, represents distinct T cell differentiation states following antigen encounter (Schietinger and Greenberg, 2014). The dysfunctional differentiation of T cells involves the transcriptional induction of essential negative regulators that inhibit T cell function (Fathman and Lineberry, 2007; Wherry and Kurachi, 2015). For instance, dysfunctional T cells that arise during certain chronic infections and cancers sustainably express various inhibitory receptors, including programmed cell death protein 1 (PD-1), CD160, lymphocyte-activation gene 3 (LAG3), B and T lymphocyte attenuator (BTLA), and cytotoxic T lymphocyte antigen 4 (CTLA-4) (Crawford et al., 2014; Schietinger et al., 2016). These receptors exert inhibitory effects on T cell function; blockade of PD-1, programmed death-ligand 1 (PD-L1), or CTLA-4 has been successfully used to treat several cancer types by reversing T cell dysfunction (Zarour, 2016).

Transcription factors T-bet, Blimp-1, NFAT, and FOXO1 regulate PD-1 expression and have been implicated in T cell exhaustion and dysfunction (Wherry and Kurachi, 2015).

Interferon regulatory factor 4 (IRF4) is a member of the IRF family of transcription factors and is preferentially expressed in hematopoietic cells. It plays essential roles in many aspects of T cell, B cell and dendritic cell differentiation and function (Huber and Lohoff, 2014; Ochiai et al., 2013; Vander Lugt et al., 2014). In T cells, IRF4 is promptly expressed within hours following TCR stimulation, and its expression level is TCR affinity dependent (Man et al., 2013). IRF4 controls the differentiation of Th2, Th9, Th17, Tfh, Treg, and cytotoxic effector $CD8^+$ T cells (Bollig et al., 2012; Brustle et al., 2007; Cretney et al., 2011; Huber et al., 2008; Staudt et al., 2010; Yao et al., 2013; Zheng et al., 2009). *Irf4*-deficient T cells exhibit a severe functional defect in T cell–mediated responses, including microbial infection, allergy, graft-versus-host reaction, and autoimmunity (Brustle et al., 2007; Grusdat et al., 2014; Huber and Lohoff, 2014; Mittrucker et al., 1997; Staudt et al., 2010).

Here we examined the role of IRF4 in transplant rejection and acceptance. We found that all fully MHC-mismatched heart allografts survived indefinitely in *Irf4*-deficient mice. This stable engraftment in *Irf4*-deficient recipients involved the progressive establishment of effector $CD4^+$ T cell dysfunction. Mechanistically, IRF4 repressed a group of previously defined molecules associated with $CD4^+$ T cell dysfunction, including PD-1 and Helios. In particular, in the absence of IRF4, chromatin accessibility and binding of Helios at PD-1 *cis*-regulatory elements were increased, resulting in enhanced PD-1 expression and $CD4^+$ T cell dysfunction. Although the dysfunctional state of *Irf4*-deficient T cells was initially reversible by blockade of PD-1–PD-L1 pathway, it progressively evolved into a “terminal” irreversible state within 30 days post-transplant. Taken together, our results revealed that IRF4 repressed the dysfunctional differentiation of $CD4^+$ T cells. Induction of T cell dysfunction by targeting IRF4 during transplantation may be a therapeutically relevant strategy for achieving transplant acceptance.

RESULTS

IRF4 is highly induced in graft-infiltrating T cells and is required for heart transplant rejection

IRF4 is a key transcription factor for translating TCR signaling into proper T cell responses (Huber and Lohoff, 2014), but its role in T cell–mediated transplant rejection remains unclear. Here we first assessed IRF4 expression in T cells in response to heart transplantation. Balb/c hearts were transplanted into fully MHC-mismatched C57BL/6 (B6) recipients. Splenocytes and graft-infiltrating cells were harvested and analyzed at 7 days post-transplant when heart allografts were rejected. We found that graft-infiltrating T cells expressed a significantly high mean fluorescence intensity (MFI) of IRF4; whilst splenic T cells from transplanted mice had a moderate increase in IRF4 expression compared to that of naïve B6 mice (Figures 1A and 1B). The majority of graft-infiltrating T cells had lost CD62L expression, but expressed T cell activation markers CD44, glucose transporter 1 (GLUT1), and CD98 (Figures S1A and S1B). Thus, IRF4 was highly expressed in graft-infiltrating T cells and was correlated to the activation status of these cells.

To investigate whether IRF4 expression in T cells plays a role in transplant rejection, we transplanted Balb/c hearts into T cell–specific IRF4 knockout (*Irf4*$^{fl/fl}$*Cd4-Cre*; B6 background) or wild-type (WT) B6 mice. None of the *Irf4*$^{fl/fl}$*Cd4-Cre* mice rejected their Balb/c heart allografts (median survival time (MST) of >100 days; n = 6), whereas WT B6 mice rejected Balb/c hearts acutely (MST = 7.17 ± 0.41 days; n=6) (Figure 1C). Histology of heart allografts harvested from *Irf4*$^{fl/fl}$*Cd4-Cre* recipient mice at days 7 and 100 post-transplant showed intact myocytes with minimal cellular infiltration and vasculopathy (Figure 1D). Hence, selective ablation of IRF4 in T cells abrogated their ability to reject heart allografts, which provides a potential prospect for achieving graft acceptance.

IRF4 is critical in T cell differentiation and accumulation of T cells in the heart allografts

To determine whether a lack of functional T cells in *Irf4*$^{fl/fl}$*Cd4-Cre* mice accounts for the graft acceptance, *Irf4*$^{fl/fl}$*Cd4-Cre* mice were adoptively transferred with 2 million WT B6 CD4$^+$ or CD8$^+$ T cells, or 20 million *Irf4*$^{-/-}$ CD4$^+$ or CD8$^+$ T cells one day prior to Balb/c heart transplantations. *Irf4*$^{fl/fl}$*Cd4-Cre* recipients transferred with 2 million WT B6 CD4$^+$ T cells acutely rejected their Balb/c heart allografts (MST=7.83 ± 0.41 days), whereas none of the *Irf4*$^{fl/fl}$*Cd4-Cre* recipients in other groups rejected the heart allografts (Figure 2A). These results indicated that in our model the lack of functional CD4$^+$ (but not CD8$^+$) T cells was essential for heart allograft acceptance, and that increasing the number of dysfunctional *Irf4*-deficient CD4$^+$ T cells failed to restore transplant rejection.

CD4$^+$CD25$^+$Foxp3$^+$ Treg cells are essential to maintain long-term allograft survival in many experimental models (Miyahara et al., 2012). To determine whether Treg cells contribute to the allograft acceptance in *Irf4*$^{fl/fl}$*Cd4-Cre* mice, we transplanted Balb/c hearts into *Irf4*$^{fl/fl}$*Cd4-Cre* mice and treated them with the PC61 anti-CD25 mAb either on days −1, 3, and 6 (induction phase of graft acceptance) or on days 50, 53, and 56 (maintenance phase), or with a control IgG on days −1, 3, and 6 post-transplant. Injection of PC61 mAb eliminated approximately 70% of CD4$^+$FoxP3$^+$ cells in peripheral blood of recipient mice one day after treatment completed (data not shown). Nevertheless, this partial Treg-cell depletion during the induction or maintenance phase did not abrogate permanent allograft survival in *Irf4*$^{fl/fl}$*Cd4-Cre* mice, which was the same as that in control IgG group (MST of >100 days; n = 5 each group) (Figure 2B).

We then focused on identifying intrinsic changes of *Irf4*-deficient T cells responsible for long-term allograft acceptance. Balb/c hearts were transplanted into *Irf4*$^{fl/fl}$*Cd4-Cre* or WT B6 mice. Before transplantation, *Irf4*$^{fl/fl}$*Cd4*-Cre mice had significantly more T cells in spleens than did WT B6 mice. At day 7 post-transplant, T cell numbers in the spleens of *Irf4*$^{fl/fl}$*Cd4-Cre* mice remained largely unchanged (similar to that in un-transplanted *Irf4*$^{fl/fl}$*Cd4-Cre* mice), while the number of splenic T cells (particularly CD8$^+$ T cells) in WT recipients was increased (Figure S1C). These results indicated that the expansion of alloreactive T cells in *Irf4*$^{fl/fl}$*Cd4*-Cre recipients was impaired. Moreover, frequencies of CD4$^+$CD62L^{low}CD44$^+$, CD8$^+$CD62L^{low}CD44$^+$, and CD4$^+$Foxp3$^+$ splenocytes from *Irf4*$^{fl/fl}$*Cd4-Cre* recipients were significantly lower than those of WT recipients (Figure S1C). CD4$^+$BCL6$^+$CXCR5$^+$ Tfh cells, CD19^{low}CD138$^+$ plasma cells, and CD19$^+$GL7$^+$PNA$^+$ germinal center B cells were absent in the spleens of *Irf4*$^{fl/fl}$*Cd4-Cre*

recipients, but were clearly detected in WT recipients at day 9 post-transplant (Figure S1D). Hence, IRF4 was essential for the induction of Tfh cell response to heart transplant.

An adoptive co-transfer model was used to further assess the intrinsic changes of *Irf4*-deficient T cells. CD45.1$^+$ WT T cells and CD45.2$^+$ *Irf4*$^{-/-}$ T cells were co-injected at a 1:1 ratio into *B6.Rag1*$^{-/-}$ mice one day before receiving Balb/c heart allografts (Figure 2C). The heart grafts were rejected between 9 to 15 days post-transplant. At day 9 post-transplant, about 30% transferred cells in spleens were *Irf4*$^{-/-}$ T cells (Figure 2D). Virtually all graft-infiltrating T cells were CD45.1$^+$ WT T cells (Figure 2E), demonstrating that *Irf4*$^{-/-}$ T cells lost the ability to infiltrate allografts. The infiltrating *Irf4*$^{-/-}$ T cells were too few to be compared with WT T cells, and thus we compared the co-injected T cells in the spleens. Both CD4$^+$ and CD8$^+$ *Irf4*$^{-/-}$ T cells did not down-regulate CD62L and barely expressed an effector marker KLRG1. CD4$^+$ *Irf4*$^{-/-}$ T cells also failed to upregulate CD44 expression (Figure 2F). In addition, the frequencies of IFN-γ– and IL-17–producing cells within CD4$^+$ *Irf4*$^{-/-}$ T cells were significantly lower than those of CD4$^+$ WT T cells (Figure 2G), and the frequency of IFN-γ–producing cells within CD8$^+$ *Irf4*$^{-/-}$ T cells was also lower than that of CD8$^+$ WT T cells (Figure 2H). Thus, IRF4 deficiency inhibited the expression of effector T cell markers and the production of signature cytokines for effector T cells in response to heart transplantation. The frequency of Foxp3$^+$ cells within CD4$^+$ *Irf4*$^{-/-}$ splenic T cells was lower than that of CD4$^+$ WT splenocytes (Figure 2G). Next, we repeated these experiments by separately transferring sorted CD4$^+$ WT, CD4$^+$ *Irf4*$^{-/-}$, CD8$^+$ WT, or CD8$^+$ *Irf4*$^{-/-}$ T cells into *B6.Rag1*$^{-/-}$ mice one day prior to BALB/c heart transplantation (Figure S2A). Ex vivo analysis of transferred cells was performed on day 9 post-transplant. Consistent with results from the co-transfer model, separately injected CD4$^+$ and CD8$^+$ *Irf4*$^{-/-}$ T cells also lost their ability to infiltrate allografts (Figure S2B). Compared to the separately transferred WT T cells in spleens, CD4$^+$ and CD8$^+$ *Irf4*$^{-/-}$ T cells largely maintained CD62L expression, barely expressed KLRG1, and produced significantly less IFN-γ (Figures S2C to S2F). CD4$^+$ *Irf4*$^{-/-}$ T cells also produced significantly less IL-17 and expressed less Foxp3 (Figure S2E). Taken together, IRF4 promoted effector T cell differentiation and infiltration into heart allografts.

IRF4 represses a group of molecules associated with CD4$^+$ T cell dysfunction

We showed above that the lack of functional CD4$^+$ T cells accounted for the graft acceptance in *Irf4*$^{fl/fl}$*Cd4-Cre* mice, and thus focus on defining the intrinsic mechanism underlying the dysfunction of *Irf4*-deficient CD4$^+$ T cells. We measured expression of inhibitory and costimulatory receptors on *Irf4*$^{-/-}$ or WT CD4$^+$ T cells one day after *in vitro* activation. Compared to WT CD4$^+$ T cells, *Irf4*$^{-/-}$ CD4$^+$ T cells expressed higher MFIs of exhaustion and anergy signatures including PD-1, CD160, CD73, and folate receptor 4 (FR4) (Martinez et al., 2012; Wherry and Kurachi, 2015), and also expressed a similar or slightly lower MFIs of BTLA and CTLA-4. Profoundly, another essential exhaustion marker, LAG-3, was significantly decreased on *Irf4*$^{-/-}$ CD4$^+$ T cells (Figure 3A).

We used microarray analysis to compare the gene expression profiles between *Irf4*$^{-/-}$ and WT CD4$^+$ T cells following two-day *in vitro* activation. Among 672 differentially expressed genes, 438 were increased in activated *Irf4*$^{-/-}$ T cells, and were significantly enriched in the

Gene Ontology (GO) categories of “negative regulation of biological process” and “negative regulation of cell activation” (Figure 3C). *Ikzf2* (encoding Helios), *Pdcd1* (encoding PD-1) and *Cd160* were among the highest upregulated genes in activated *Irf4*$^{-/-}$ CD4^{+} T cells when compared to activated WT CD4^{+} T cells (Figure 3B), which were confirmed by quantitative real-time PCR (Figure 3D). Helios is a signature protein for T cell dysfunction (Crawford et al., 2014; Singer et al., 2016). We found that Helios protein was absent in activated WT CD4^{+} T cells, but was expressed in more than 50% activated *Irf4*$^{-/-}$ CD4^{+} T cells (Figure 3E). Collectively, IRF4 repressed a group of previously defined molecules associated with CD4^{+} T cell dysfunction.

IRF4 represses CD4^{+} T cell expression of PD-1

Given that *Pdcd1* was among the highest upregulated genes in *Irf4*$^{-/-}$ versus WT CD4^{+} T cells after activation, we aimed to understand the regulation of PD-1 expression by IRF4. We observed that PD-1 expression on *Irf4*$^{-/-}$ CD4^{+} T cells was progressively increased from day 0 to day 3 upon *in vitro* activation (Figure 4A), and was much higher than that of co-cultured CD45.1^{+} WT CD4^{+} T cells (Figure 4B). To further examine the role of IRF4 in PD-1 expression, activated *Irf4*$^{-/-}$ CD4^{+} T cells were transduced with a retroviral vector expressing IRF4-green fluorescent protein (GFP) or a control vector expressing just GFP. As shown in Figure 4C, transduction of IRF4 into activated *Irf4*$^{-/-}$ CD4^{+} T cells (detected by GFP expression) led to a marked inhibition of PD-1 expression when compared with GFP control transduction. Thus, IRF4 expression in activated T cells mediated repression of PD-1.

To determine how IRF4 represses PD-1 expression, we performed Chromatin Immunoprecipitation (ChIP) analysis. In activated WT CD4^{+} T cells (expressing IRF4), we did not detect specific enrichment of IRF4 at the putative binding sites upstream of *Pdcd1* or at a set of known *cis*-elements of the *Pdcd1* gene, including two upstream conserved regions (*CR-B* and *CR-C*) as well as two regions located −3.7 and +17.1 kb from the *Pdcd1* transcription start site (Bally et al., 2016) (Figure S3). These data suggested that the repression effect of IRF4 on PD-1 expression was unlikely related to its transcriptional activity. We next investigated whether histone modifications are involved in the regulation of PD-1 expression by IRF4. As shown in Figure 4D, H3 acetylation (H3Ac) was significantly increased at the −3.7 site and the *CR-B* and *CR-C* regions, whereas H4 acetylation (H4Ac) and H3 lysine 4 trimethylation (H3K4me3) were markedly increased at the −3.7 site and the *CR-C* region in activated *Irf4*$^{-/-}$ CD4^{+} T cells compared with those in activated WT CD4^{+} T cells. H3Ac, H4Ac, and H3K4me3 are all active histone marks. The expression of a repressive histone mark, H3 lysine 9 trimethylation (H3K9me3), displayed no changes at the *cis*-elements of *Pdcd1* in *Irf4*$^{-/-}$ relative to WT CD4^{+} T cells. Therefore, IRF4 deficiency in activated CD4^{+} T cells induced an active chromatin state at the critical *cis*-elements of *Pdcd1*, correlating to the elevated PD-1 expression.

In activated *Irf4*$^{-/-}$ CD4^{+} T cells, most PD-1^{hi} cells were Helios positive (Figure 4E). We thus investigated whether Helios regulates PD-1 expression. This possibility was supported by a ChIP assay, which detected the binding of Helios to the *cis*-elements of *Pdcd1* in activated *Irf4*$^{-/-}$ CD4^{+} T cells (Figure 4F). Furthermore, activated WT CD4^{+} T cells (with

minimal Helios expression) were transduced with a retroviral vector expressing Helios-GFP or just GFP. We found that transduction of Helios into activated WT $CD4^+$ T cells resulted in a marked increase of PD-1 expression when compared with GFP control transduction (Figure 4G). Activated *Irf4*$^{-/-}$ $CD4^+$ T cells (with Helios expression) were also transduced with a retroviral vector co-expressing GFP and short hairpin RNA (shRNA) sequences for Helios (sh-Helios) or expressing GFP alone (sh-Ctrl). As indicated by GFP^+ cells, transduction with sh-Helios decreased PD-1 expression in *Irf4*$^{-/-}$ $CD4^+$ T cells (Figure 4H). Thus, Helios promoted PD-1 expression. Taken together, IRF4 deletion progressively increased PD-1 expression on activated T cells, which was associated with the increased chromatin accessibility and Helios binding to PD-1 *cis*-regulatory elements.

Dysfunctional state of *Irf4*-deficient T cells is initially reversible by PD-L1 blockade but it progressively develops into an irreversible state

TCR-transgenic TEa $CD4^+$ T cells (B6 background) recognize a Balb/c I-Eα allopeptide presented by B6 APCs; mice containing only TEa T cells were able to reject Balb/c skin allografts (Gupta et al., 2011). We found that adoptive transfer of WT TEa but not *Irf4*$^{-/-}$ TEa cells induced rejection of Balb/c hearts in *Irf4*$^{fl/fl}$*Cd4-Cre* recipients (Figure 5A). To determine whether immune checkpoint PD-1 contributes to the dysfunction of alloantigen-specific *Irf4*-deficient $CD4^+$ T cells in transplantation, we assessed PD-1 expression on *Irf4*$^{-/-}$ TEa versus WT TEa cells by transferring and tracking these cells in $CD45.1^+$ B6 congenic mice. As shown in Figure 5B, $CD45.1^+$ B6 mice were transferred with either $CD45.2^+$ WT TEa or $CD45.2^+$ *Irf4*$^{-/-}$ TEa cells on day −1, and were transplanted with Balb/c hearts or left un-transplanted on day 0. Splenocytes were analyzed on day 6 (Figure 5B). In $CD45.1^+$ B6 mice without Balb/c heart grafting, TEa $CD4^+$ T cells neither proliferated nor expressed PD-1. In heart transplanted mice, *Irf4*$^{-/-}$ TEa cells exhibited higher PD-1 expression and a lower proliferation rate than did WT TEa cells (Figure 5B). Thus, IRF4 deficiency promoted PD-1 expression on alloantigen-specific T cells, which was associated with decreased cell proliferation. Intracellular CTLA-4 expression was also detectable in WT and *Irf4*$^{-/-}$ TEa cells in transplanted groups, and WT TEa cells expressed more intracellular CTLA-4 than that of *Irf4*$^{-/-}$ TEa cells (Figure 5B).

To investigate the influence of PD-1 on permanent cardiac allograft survival in *Irf4*$^{fl/fl}$*Cd4-Cre* recipient mice, we transplanted Balb/c hearts into *Irf4*$^{fl/fl}$*Cd4-Cre* mice and treated them with anti-PD-L1 mAb alone, anti-CTLA-4 mAb alone, or both mAbs on days 0, 3, and 5 post-transplant. The control *Irf4*$^{fl/fl}$*Cd4-Cre* recipient mice were treated with rat IgG. Three of five heart allografts in anti-PD-L1 mAb-treated recipients were rejected within 35 days, whereas all allografts survived more than 100 days in recipient mice treated with anti-CTLA-4 mAb alone or rat IgG. By contrast, all six heart allografts in recipient mice treated with both anti-PD-L1 and anti-CTLA-4 mAbs were rejected on days 7–8 post-transplant (Figure 5C). Analysis of splenocytes at day 7 post-transplant revealed that anti-PD-L1 plus anti-CTLA-4 treatment increased expression of proliferation marker Ki67, metabolic activation makers CD98 and CD71, and effector cytokine IFN-γ of *Irf4*-deficient $CD4^+$ T cells (Figure S4). Anti-PD-L1 plus anti-CTLA-4 treatment increased Treg cell frequency (Figure S4), but those *Irf4*-deficient Treg cells displayed impaired suppressive function *in vitro*. Indeed, the suppressive function of Treg cells from all *Irf4*$^{fl/fl}$*Cd4-Cre* mice (including

non-transplanted, or transplanted groups treated with control IgG or immune checkpoint blockade) was impaired compared to those from naïve WT B6 mice (Figure 5D and 5E). Depletion of $CD4^+$ but not $CD8^+$ T cells abrogated the capability of anti-PD-L1 plus anti-CTLA-4 treatment in restoring heart allograft rejection in *Irf4*$^{fl/fl}$*Cd4-Cre* recipients (Figure 5F and 5G). Therefore, in this checkpoint-blockade model, the reversal of $CD4^+$ (but not $CD8^+$) T cell dysfunction was essential for restoring transplant rejection.

We also transplanted Balb/c hearts into *Irf4*$^{fl/fl}$*Cd4-Cre* mice and treated them with both 200 μg anti-PD-L1 and 200 μg anti-CTLA-4 mAbs starting from day 0 (on days 0, 3, and 5), day 7 (on days 7, 10, and 12), or day 30 (on days 30, 33, and 35) post-transplant. Immune checkpoint blockade starting from day 7 was not as potent as the treatment group starting from day 0, but still restored rejection of four of six heart allografts. Immune checkpoint blockade starting from day 30 post-transplant did not restore allograft rejection in *Irf4*$^{fl/fl}$*Cd4-Cre* mice, and all five allografts survived more than 100 days (Figure 5H). Taken together, PD-1 was highly expressed by alloantigen-specific *Irf4*-deficient T cells; blockade of its ligand, PD-L1, was capable of reversing the initial dysfunctional state of *Irf4*-deficient T cells. Moreover, within 30 days post-transplant, *Irf4*-deficient T cells progressed from the reversible dysfunctional state into a “terminal” irreversible state.

Another approach that has been successfully applied in restoring transplant rejection in *Irf4*$^{fl/fl}$*Cd4-Cre* recipients was to transfer IRF4 re-introduced *Irf4*$^{-/-}$ $CD4^+$ T cells. *Irf4*$^{-/-}$ $CD4^+$ T cells were stimulated with allogenic Balb/c splenic DCs and IL-2 for 3 days, followed by transduction with IRF4-GFP or GFP-control retrovirus for 1 day. Histogram in Figure 5I shows the transduction efficacy of IRF4-GFP. *Irf4*$^{fl/fl}$*Cd4*-Cre recipients injected with one million IRF4 re-introduced (but not GFP-control transduced) *Irf4*$^{-/-}$ $CD4^+$ T cells acutely rejected heart allografts within 6 days (Figure 5J). Therefore, IRF4 re-introduction in *Irf4*$^{-/-}$ $CD4^+$ T cells after the 3-day activation period reversed their dysfunction. This finding separates the role of IRF4 in early $CD4^+$ T cell activation from its role in subsequent dysfunctional development.

Checkpoint blockade reverses the initial dysfunction of *Irf4*-deficient $CD4^+$ T cells by restoring their ability to undergo proliferation and secrete IFN-γ

We used the TEa cell transfer model to further characterize how checkpoint blockade reverses the initial dysfunction of alloantigen-specific *Irf4*$^{-/-}$ $CD4^+$ T cells. $CD45.1^+$ B6 mice were transferred with $CD45.2^+$ *Irf4*$^{-/-}$ TEa cells on day −1, transplanted with Balb/c hearts on day 0, and treated with either rat IgG (IgG group) or anti-PD-L1 plus anti-CTLA-4 mAbs (P+C group) on days 0, 3, and 5. In addition, $CD45.1^+$ B6 mice transferred with $CD45.2^+$ WT TEa cells were transplanted with Balb/c hearts or left un-transplanted. Splenocytes were analyzed on day 6 (Figures 6A and S5A). We found that checkpoint blockade affected the *Irf4*$^{-/-}$ TEa cells in transplanted mice by restoring cell number, proliferation (indicated by Ki67), metabolic activation (indicated by CD98 and CD71), and IFN-γ production (Figures 6B and 6C). CD62L and CD44 expression, BCL6 and CXCR5 expression, and IL-17 production of *Irf4*$^{-/-}$ TEa cells were less affected by checkpoint blockade (Figure S5B), suggesting that *Irf4*$^{-/-}$ TEa cells exposed to checkpoint blockade remained different from WT TEa cells. Taken together, the combined blockade of PD-L1

and CTLA-4 was extremely effective to reverse the initial dysfunction of *Irf4*-deficient $CD4^+$ T cells by restoring their ability to undergo proliferation and secrete IFN-γ.

Pharmacological inhibition of IRF4 reduces Th1 and Th17 cell differentiation, abrogates EAE development and prolongs heart allograft survival

IRF4 deletion led to $CD4^+$ T cell dysfunction in transplantation, suggesting the therapeutic potential of IRF4 inhibition in preventing allograft rejection. To identify approaches for IRF4 inhibition, we examined the effects of cytokines and small-molecule inhibitors on IRF4 expression upon *in vitro* $CD4^+$ T cell activation. None of the tested cytokines modulated the IRF4 expression in activated $CD4^+$ T cells, though several of them altered the expression of a binding partner of IRF4, basic leucine zipper transcription factor ATF-like (BATF) (Figure S6A). Many tested inhibitors induced T cell death upon *in vitro* activation and reduced IRF4 expression (data not shown). Nevertheless, by gating on the living $CD4^+$ T cells, a MEK1/2 inhibitor trametinib most potently reduced IRF4 expression in a dose-dependent manner (Figures 7A and S6). Similar to *Irf4*-deficient $CD4^+$ T cells, the majority of the trametinib-treated WT $CD4^+$ T cells expressed Helios (which was not expressed by most DMSO-treated WT $CD4^+$ T cells). Trametinib also increased PD-1 expression on WT $CD4^+$ T cells, and most PD-1^{hi} cells were Helios positive. For activated *Irf4*-deficient $CD4^+$ T cells, PD-1 and Helios were already highly expressed, and trametinib barely affects their expressions (Figure S6E). Moreover, 100 nM trametinib was sufficient to inhibit $CD4^+$ T cell proliferation as well as Th1 and Th17 cell differentiation, but promoted the differentiation of inducible Treg cells (Figures 7B and 7C).

Th1 and Th17 cells contribute to the pathogenesis of experimental autoimmune encephalomyelitis (EAE) (Rangachari and Kuchroo, 2013). We thus investigated whether transient trametinib treatment would affect EAE development. Female WT mice were immunized with the MOG35-55 peptide and treated with corn oil or 3mg/kg trametinib every other day from day 0 to day 12. Control mice treated with corn oil developed EAE with a mean disease onset of 12.0 ± 0.47 days post-immunization. By contrast, mice treated with trametinib were absolutely resistant to EAE and exhibited no incidence of disease, indicated by definitely absence in the loss of motor function or paralysis throughout the entire period of observation (Figure 7D). $CD4^+$ T cell infiltration in the brain was dramatically decreased in mice treated with trametinib compared with corn oil controls, and the expression of cytokines GM-CSF, IFN-γ, IL-17, and Foxp3 by brain infiltrating $CD4^+$ T cells was significantly decreased (Figures 7E, S7A and S7B). The frequency of IL-17^+ $CD4^+$ T cells in the periphery was also lower in trametinib-treated mice than that of control mice (Figure S7C).

We then examined whether trametinib is effective to prolong allograft survival. WT B6 mice were transplanted Balb/c hearts and treated with corn oil or 3mg/kg trametinib every other day from day 0 to day 12. Trametinib-treated recipient mice displayed prolonged heart allograft survival (MST = 13.17 ± 0.75 days) compared with corn oil controls (MST = 7.33 ± 0.52 days) (Figure 7F). A TEa cell transfer model was applied to determine whether or not trametinib affects the PD-1 and Helios expressions of alloantigen-specific $CD4^+$ T cells. $CD45.1^+$ B6 mice were transferred with $CD45.2^+$ TEa cells on day −1, transplanted with

Balb/c hearts on day 0, and treated with corn oil or 3mg/kg trametinib on day 0, 2, 4, and 6. On day 7 post-transplant, splenocytes were analyzed. We found that trametinib promoted PD-1 and Helios expression on TEa cells in transplanted mice (Figures 7G). Collectively, these data indicated that trametinib effectively reduced IRF4 expression in activated T cells, inhibited Th1 and Th17 cell differentiation, abrogated EAE development, and prolonged heart allograft survival.

DISCUSSION

The transcriptional programs regulating allogeneic T cell responses and subsequent transplant outcomes (rejection versus acceptance) have not been adequately explored. In the present work, we found that all heart allografts survived indefinitely in mice when IRF4 was deleted in T cells. Further mechanistic investigation revealed that IRF4 repressed the expression of a group of molecules associated with T cell dysfunction, including PD-1 and Helios. Thus, *Irf4*-deficient $CD4^+$ T cells displayed increased expression of these molecules and underwent differentiation to a dysfunctional fate. The initial dysfunctional state of *Irf4*-deficient T cells was reversible by immune checkpoint blockade, but its late dysfunctional state was irreversible. Therefore, IRF4 is a key transcriptional determinant that dictates effector T cell fate decisions; IRF4 deletion leads to the progressive establishment of $CD4^+$ T cell dysfunction and long-term allograft survival.

We found that all Balb/c heart allografts survived indefinitely in $Irf4^{fl/fl}$*Cd4-Cre* mice that were not treated with any immunosuppressive therapies. Of note, deficiency of several other molecules also allows T cell development but impairs T cell function, such as BATF, signal transducer and activator of transcription 3 (STAT3), nuclear factor κB subunit c-Rel, and IL2-inducible T cell kinase (Itk) (Murphy et al., 2013; Notarangelo, 2013). BATF and STAT3 are also required for Th17 and Tfh cell differentiation. We have transplanted Balb/c hearts into $Batf^{-/-}$, $Irf4^{-/-}$, and $Stat3^{fl/fl}$*Cd4-Cre* mice (data not shown). Only $Irf4^{-/-}$ and $Irf4^{fl/fl}$*Cd4-Cre* recipient mice permanently accepted Balb/c hearts. Thus, lack of Th17 and Tfh cell differentiation is not sufficient to completely explain the severe dysfunction of *Irf4*-deficient T cells. c-Rel and Itk have been shown to control IRF4 expression in lymphocytes (Grumont and Gerondakis, 2000; Nayar et al., 2012). The role of these two molecules in transplantation was either unknown or less significant than that of IRF4 observed in this study (Yang et al., 2002).

Previous reports showed that *Irf4*-deficient T cells do not expand properly upon antigen stimulation (Mahnke et al., 2016; Man et al., 2013). We also found that T cell frequencies in the spleens of $Irf4^{fl/fl}$*Cd4-Cre* mice remained largely unchanged at day 7 post-transplantation. Thus, the expansion of alloreactive T cells in those recipients was impaired. We further found that alloantigen-specific $Irf4^{-/-}$ $CD4^+$ T cells responded to heart allografts and expanded as indicated by CTV labeling, though they were generally found to be 2 to 4-fold less than the frequency of expanded WT alloantigen-specific $CD4^+$ T cells. It took as few as 2 million transferred WT $CD4^+$ T cells to induce acute rejection of heart allografts in $Irf4^{fl/fl}$*Cd4-Cre* recipients. By contrast, whole endogenous population of $Irf4^{fl/fl}$*Cd4-Cre* T cells plus 20 million transferred *Irf4*-deficient $CD4^+$ T cells failed to reject heart allografts in $Irf4^{fl/fl}$*Cd4-Cre* recipients. These results suggested that reduced expansion of *Irf4*-deficient

CD4$^+$ T cells was not the only reason why *Irf4*$^{fl/fl}$*Cd4-Cre* recipients permanently accepted their heart allografts.

A major mechanistic finding in this study was that IRF4 repressed the expression of essential molecules associated with T cell dysfunction. Hence, IRF4 deletion in activated CD4$^+$ T cells led to increased expression of PD-1, Helios, PLAGL1, CD160, CD73, and FR4, which are characteristic markers of dysfunctional T cells (Crawford et al., 2014; Fathman and Lineberry, 2007; Martinez et al., 2012; Wherry and Kurachi, 2015). Given that PD-1 is a key immune checkpoint molecule implicated in T cell dysfunction, we investigated the regulation of PD-1 expression by IRF4. In the absence of IRF4, activated CD4$^+$ T cells induced an active chromatin state at the critical *cis*-elements of *Pdcd1*, as well as the robust Helios expression. We then found that Helios bound to *cis*-elements of *Pdcd1* and promoted PD-1 expression. Helios has been shown to be highly expressed by natural Treg cells, exhausted T cells, and tolerated T cells (Crawford et al., 2014; Kim et al., 2015; Ross et al., 2014; Singer et al., 2016). It will be interesting to further define whether Helios sustains PD-1 expression in those cells. Transcription factors NFAT1, T-bet, FoxO1, and Blimp1 have also been shown to regulate PD-1 expression (Wherry and Kurachi, 2015), but the connection between IRF4 and these molecules on *Pdcd1* transcription will require further investigation.

We attributed the initial dysfunction of *Irf4*-deficient T cells in transplantation to the presence of inhibitory checkpoints. PD-1 was highly expressed on alloantigen-specific *Irf4*-deficient T cells; blockade of its ligand, PD-L1, during the initial days post-transplant was capable of restoring the anti-allograft function of *Irf4*-deficient T cells. Activated *Irf4*-deficient T cells also expressed intracellular CTLA-4, though at a relatively low expression compared to that of activated WT T cells. Transient blockade of PD-L1 plus CTLA-4 during the initial days post-transplant synergistically and completely rescued the anti-allograft function of *Irf4*-deficient T cells by restoring their ability to undergo proliferation and IFN-γ production. Thus, these two major inhibitory checkpoints operated as non-redundant pathways to mediate the dysfunction of *Irf4*-deficient T cells, likely due to their distinct mechanisms of action (Baumeister et al., 2016; Larkin et al., 2015; Postow et al., 2015). However, blockade of PD-L1 plus CTLA-4 starting from day 30 post-transplant did not induce heart allograft rejection in *Irf4*$^{fl/fl}$*Cd4-Cre* recipients. Therefore, a progressive process must exist to establish the irreversible dysfunctional state of *Irf4*-deficient T cells.

A very high proportion of polyclonal WT T cells (~0.1–10%) in transplant recipients are able to recognize and respond to intact allogeneic MHC on donor APCs (termed direct allorecognition) or donor MHC peptides presented by recipient APCs (termed indirect allorecognition) (Lechler et al., 2005; Rogers and Lechler, 2001). All these unique characteristics of allogeneic T cell response contribute significantly to allograft rejection. TEa CD4$^+$ T cells only recognize a Balb/c donor I-Eα allopeptide through the indirect allorecognition pathway, and may be less effective to mediate transplant rejection compared to that of polyclonal WT CD4$^+$ T cells. We thus adoptively transferred 20 million WT TEa and *Irf4*$^{-/-}$ TEa cells into *Irf4*$^{fl/fl}$*Cd4-Cre* recipients to investigate their ability to reject heart allografts. WT TEa but not *Irf4*$^{-/-}$ TEa cells mediated heart allograft rejection. Therefore, the TEa cell transfer model is valuable to track the *in vivo* phenotypic changes of

alloreactive $CD4^+$ T cells associated with IRF4 deficiency and immune checkpoint blockade.

Recent reports indicated that in patients with stable function of transplanted kidneys but also developed metastatic cancer, PD-1 blockade was used to treat cancer. Unfortunately, PD-1 blockade triggered acute rejection of the transplanted kidneys (Alhamad et al., 2016; Lipson et al., 2016). Given that the late dysfunctional state of *Irf4*-deficient T cells was irreversible by checkpoint blockade, it would be interesting to know whether pharmaceutical IRF4 inhibition could be a potential therapeutic approach for transplantation. We found that trametinib was an effective inhibitor that diminished IRF4 expression in activated $CD4^+$ T cells. Transient trametinib treatment abolished EAE development and prolonged allograft survival. Although further investigations are required to define the immune mechanism of action of trametinib, these results demonstrated the feasibility of targeting IRF4 expression for eliminating undesired T cell responses.

In summary, IRF4 restrained the dysfunctional differentiation of $CD4^+$ T cells, representing a novel role for IRF4 in linking TCR signaling to $CD4^+$ T cell fates. Moreover, we introduced the concept of T cell dysfunction, which is mainly documented in chronic viral infection and tumor models, into research aiming to eliminate undesired T cells responses, such as transplant rejection and autoimmunity. Induction of T cell dysfunction by targeting IRF4 represents a potential therapeutic strategy for treatment of transplant rejection and autoimmune disorders.

STAR METHODS

Detailed methods are provided in the online version of this paper and include the following:

KEY RESOURCES TABLE

REAGENT or RESOURCE	SOURCE	IDENTIFIER
Antibodies		
Anti-IRF4 (polyclonal M-17)	Santa Cruz	Cat#sc-6059; RRID:AB_2127145
Donkey anti-Goat IgG, Alexa Fluor 488	Thermo Fisher	Cat#A-11055; RRID:AB_2534102
Donkey anti-Goat IgG, Alexa Fluor 647	Thermo Fisher	Cat#A-21447; RRID:AB_2535864
Anti-CD3 (clone 145-2C11)	Thermo Fisher	Cat#45-0031-82; RRID:AB_1107000
Anti-CD45 (clone 30-F11)	BioLegend	Cat#103116; RRID:AB_312981
Anti-CD45.1 (clone A20)	BioLegend	Cat#110716; RRID:AB_313505
Anti-CD4 (clone GK1.5)	BioLegend	Cat#100422; RRID:AB_312707
Anti-CD8 (clone 53-6.7)	BioLegend	Cat#100725; RRID:AB_493425
Anti-CD62L (clone MEL-14)	BioLegend	Cat#104406; RRID:AB_313093
Anti-CD44 (clone IM7)	Thermo Fisher	Cat#56-0441-82; RRID:AB_494011
Anti-CD25 (clone PC61.5)	Thermo Fisher	Cat#17-0251-82; RRID:AB_469366
Anti-KLRG1 (clone MAFA)	BioLegend	Cat#138408; RRID:AB_10574313
Anti-IFNγ (clone XMG1.2)	BioLegend	Cat#505808; RRID:AB_315402

REAGENT or RESOURCE	SOURCE	IDENTIFIER
Anti-IL17A (clone TC11-18H10.1)	BioLegend	Cat#506904; RRID:AB_315464
Anti-TNFα (clone MP6-XT22)	Thermo Fisher	Cat#12-7321-82; RRID:AB_466199
Anti-Foxp3 (clone FJK-16s)	Thermo Fisher	Cat#12-5773-82; RRID:AB_465936
Anti-IL-4 (clone 11B11)	BioLegend	Cat#504104; RRID:AB_315318
Anti-Perforin (clone eBioOMAK-D)	Thermo Fisher	Cat#12-9392-82; RRID:AB_466243
Anti-Granzyme B (clone GB11)	BioLegend	Cat#515406; RRID:AB_2566333
Anti-PD-1 (clone 29F.1A12)	BioLegend	Cat#135210; RRID:AB_2159183
Anti-CD160 (clone 7H1)	BioLegend	Cat#143004; RRID:AB_10960743
Anti-CD73 (clone TY/11.8)	BioLegend	Cat#127209; RRID:AB_11219400
Anti-FR4 (clone TH6)	BioLegend	Cat#125107; RRID:AB_1236541
Anti-BTLA (clone 6A6)	BioLegend	Cat#139106; RRID:AB_10613297
Anti-CTLA-4 (clone UC10-4B9)	Thermo Fisher	Cat#17-1522-82; RRID:AB_2016700
Anti-LAG-3 (clone C9B7W)	BioLegend	Cat#125209; RRID:AB_10639935
Anti-PD-L1 (clone MIH5)	Thermo Fisher	Cat#12-5982-82; RRID:AB_466089
Anti-2B4 (clone m2B4 (B6)458.1)	BioLegend	Cat#133507; RRID:AB_1626231
Anti-TIM3 (clone 8B.2C12)	Thermo Fisher	Cat#12-5871-81; RRID:AB_465976
Anti-CD69 (clone H1.2F3)	Thermo Fisher	Cat#12-0691-82; RRID:AB_465732
Anti-GITR (clone DTA-1)	BioLegend	Cat#126309; RRID:AB_1089132
Anti-4-1BB (clone 17B5)	Thermo Fisher	Cat#12-1371-81; RRID:AB_465863
Anti-CD226 (clone 10E5)	BioLegend	Cat#128805; RRID:AB_1186120
Anti-Helios (clone 22F6)	Thermo Fisher	Cat#12-9883-42; RRID:AB_2572758
Anti-CD45.2 (clone 104)	BioLegend	Cat#109822; RRID:AB_493731
Anti-TCR Vα2 (clone B20.1)	BioLegend	Cat#127806; RRID:AB_1134188
Anti-TCR Vβ6 (clone RR4-7)	Thermo Fisher	Cat#46-5795-82; RRID:AB_11150054
Anti-Ki-67 (clone SolA15)	Thermo Fisher	Cat#25-5698-82; RRID:AB_11220070
Anti-ICOS (clone C398.4A)	Thermo Fisher	Cat#12-9949-81; RRID:AB_466277
Anti-CD71 (clone RI7217)	BioLegend	Cat#113812; RRID:AB_2203382
Anti-CD98 (clone RL388)	BioLegend	Cat#128207; RRID:AB_1186107
Anti-GLUT1 (clone SPM498)	Abcam	Cat#ab40084; RRID:AB_2190927
Anti-IL17F (clone 9D3.1C8)	BioLegend	Cat#517003; RRID:AB_10578083
Anti-TCR β (clone H57-597)	BioLegend	Cat#109222; RRID:AB_893625
Anti-GM-CSF (clone MP1-22E9)	Thermo Fisher	Cat#12-73331-82; RRID:AB_466205
Anti-BCL-6 (clone K112-91)	BD Biosciences	Cat#561522; RRID:AB_10717126
Anti-CXCR5 (clone 2G8)	BD Biosciences	Cat#551960; RRID:AB_394301
APC Streptavidin	BD Biosciences	Cat# 554067; RRID:AB_10050396
BV421 Streptavidin	BD Biosciences	Cat#563259; RRID:AB_2687865
Anti-CD138 (clone 281-2)	BioLegend	Cat#142514; RRID:AB_2562198
Anti-CD19 (clone 6D5)	BioLegend	Cat#115510; RRID:AB_313645
Anti-GL7 (clone GL7)	BioLegend	Cat#144614; RRID:AB_2563292

REAGENT or RESOURCE	SOURCE	IDENTIFIER
Fluorescein labeled Peanut Agglutinin	Vector Lab	Cat#FL-1071; RRID:AB_2315097
Anti-IL-10 (clone JES5-16E3)	BioLegend	Cat#505014; RRID:AB_493511
Anti-IL-2 (clone JES6-5H4)	BioLegend	Cat#503818; RRID:AB_528931
Anti-IL-13 (clone eBio13A)	Thermo Fisher	Cat#46-7133-82; RRID:AB_11218496
Anti-BATF (clone D7C5)	Cell Signaling	Cat#8638S; RRID:AB_11141425
Anti-β-Actin (clone 8H10D10)	Cell Signaling	Cat#12262; RRID:AB_2566811
Anti-rabbit IgG, HRP-linked	Cell Signaling	Cat#7074; RRID:AB_2099233
Anti-mouse IgG, HRP-linked	Cell Signaling	Cat#7076; RRID:AB_330924
Anti-goat IgG, HRP-linked	Santa Cruz	Cat#sc-2768; RRID:AB_656964
Anti-Histone H3K9me3 (clone MABI 0319)	Active Motif	Cat#61013; RRID:AB_2687870
Anti-H3K4me3	Millipore	Cat#17-678; RRID:AB_1977250
Anti-H3Ac	Active Motif	Cat#39139; RRID:AB_2687871
Anti-H4Ac	Active Motif	Cat#39925; RRID:AB_2687872
Anti-Helios	Santa Cruz	Cat#sc-9864; RRID:AB_2124965
Rabbit IgG control	Santa Cruz	Cat#sc-2027; RRID:AB_737197
*In Vivo*MAb anti-PD-L1(clone 10F.9G2)	BioXcell	Cat#BE0101; RRID:AB_10949073
*In Vivo*MAb anti-CTLA-4 (clone 9D9)	BioXcell	Cat#BE0164; RRID:AB_10949609
*In Vivo*MAb anti-CD4 (clone GK1.5)	BioXcell	Cat#BE0003-1; RRID:AB_1107636
*In Vivo*MAb anti-CD8α (clone 53-6.7)	BioXcell	Cat#BE0004-1; RRID:AB_1107671
*In Vivo*MAb anti-CD25 (clone PC-61.5.3)	BioXcell	Cat#BE0012; RRID:AB_1107619
Rat IgG2b isotype control	BioXcell	Cat#BE0090; RRID:AB_1107780
PE anti-CD3ε (clone 145-2C11)	BioLegend	Cat#100308; RRID:AB_312673
Purified anti-CD3ε (clone 145-2C11)	BioLegend	Cat#100314; RRID:AB_312679
Bacterial and Virus Strains		
pMYs-IRES-GFP Retroviral Vector	Cell Biolabs	Cat#RTV-021
Plat-E Retroviral Packaging Cell Line	Cell Biolabs	Cat#RV-101
RNAi-Ready pSIREN-RetroQ-ZsGreen1	Clontech	Cat#632455
Chemicals, Peptides, and Recombinant Proteins		
Human TGF-β1	PeproTech	Cat#100-21
Murine IL-6	PeproTech	Cat#216-16
Murine IL-1β	PeproTech	Cat#211-11B
Mouse IL-23	R&D	Cat#1887-ML-010
Murine IL-12	PeproTech	Cat#210-12
Murine IL-2	PeproTech	Cat#212-12
Trametinib (GSK1120212)	Selleck	Cat#S2673; CAS:871700-17-3
Phorbol 12-myristate 13-acetate	Sigma-Aldrich	Cat#P8139; CAS:16561-29-8
Ionomycin	Sigma-Aldrich	Cat#I3909; CAS:56092-82-1
Mitomycin C	Fisher Scientific	Cat#BP25312; CAS:50-07-7
Critical Commercial Assays		

REAGENT or RESOURCE	SOURCE	IDENTIFIER
Zombie Aqua™ Fixable Viability Kit	BioLegend	Cat#423102
CellTrace™ Violet Cell Proliferation Kit	Thermo Fisher	Cat#C34557
Foxp3/Transcription Factor Staining Set	Thermo Fisher	Cat#00-5523-00
BD Cytofix/Cytoperm™ with GolgiStop	BD Biosciences	Cat#554715
Dynabeads Untouched Mouse T Cells Kit	Thermo Fisher	Cat#11413D
Hooke Kit™ MOG_{35-55}/CFA Emulsion PTX	Hooke Lab	Cat#EK-0113
Dynabeads Untouched Mouse CD4 Kit	Thermo Fisher	Cat#11416D
Dynabeads Mouse CD4+CD25+ Treg Kit	Thermo Fisher	Cat#11463D
RNeasy Mini Kit	Qiagen	Cat#74106
iScript™ Reverse Transcription Supermix	Bio-rad	Cat#1708841
EZ-ChIP™	Millipore	Cat#17-371
Low Input Quick Amp Labeling, one-color	Agilent	Cat#5190-2305
SurePrint G3 Mouse GE v2 8×60K Kit	Agilent	Cat#G4852B
Pan Dendritic Cell Isolation Kit, mouse	Miltenyi Biotec	Cat#130-100-875
Anti-PE MicroBeads	Miltenyi Biotec	Cat#130-048-801
Deposited Data		
Microarray	This paper	GEO: GSE83283
Experimental Models: Organisms/Strains		
Mouse: C57BL/6	Jackson Lab	JAX: 000664
Mouse: BALB/c	Jackson Lab	JAX: 000651
Mouse: CD4-Cre	Jackson Lab	JAX: 022071
Mouse: *Irf4*(fl/fl): B6.129S1-Irf4tm1Rdf/J	Jackson Lab	JAX: 009380
Mouse: *Rag1*−/−	Jackson Lab	JAX: 002216
Mouse: B6.SJL CD45.1	Jackson Lab	JAX: 002014
Mouse: TEa: B6.Cg-Tg(Tcra,Tcrb)3Ayr/J	Jackson Lab	JAX: 005655
Mouse: Foxp3GFP: B6.Cg-Foxp3tm1Mal/J	Jackson Lab	JAX: 018628
Mouse: *Irf4*−/−	Ochiai et al., 2013	N/A
Oligonucleotides		
ShRNA targeting sequence for *Ikzf2*: GCAGGTCATGAGTCACCATGT	This paper	N/A
ChIP-PCR Primers, see Figure S3	This paper	N/A
Recombinant DNA		
Plasmid: IRF4-GFP	This paper	N/A
Plasmid: Helios-GFP	This paper	N/A
Plasmid: sh-Helios	This paper	N/A
Software and Algorithms		
FlowJo v10	Tree Star Inc	https://www.flowjo.com/
Subio Platform	Subio Inc	https://www.subioplatform.com/
PANTHER	Thomas lab, University of	http://www.pantherdb.org/panther/ontologies.jsp

REAGENT or RESOURCE	SOURCE	IDENTIFIER
	Southern California	
Prism version 7.0a	GraphPad Software	http://www.graphpad.com/scientific-software/prism/

CONTACT FOR REAGENT AND RESOURCE SHARING

Further information and request for resources and reagents should be directed to and will be fulfilled by the Lead Contact, Wenhao Chen (wchen@houstonmethodist.org).

EXPERIMENTAL MODEL AND SUBJECT DETAILS

Mice—*Cd4*-Cre, *Irf4*$^{flox/flox}$, *Rag1*$^{-/-}$, B6.SJL CD45.1 congenic, TEa TCR transgenic, *Foxp3gfp* reporter, Balb/c, and C57BL/6 (B6) mice were purchased from Jackson Laboratory (Bar Harbor, MA). *Irf4*$^{-/-}$ mice has been previously described (Mittrucker et al., 1997; Ochiai et al., 2013). *Irf4*$^{flox/flox}$ mice were crossed to *Cd4*-Cre mice to create *Irf4*$^{fl/fl}$*Cd4*-Cre mice. TEa mice were crossed to *Irf4*$^{-/-}$ mice to create *Irf4*$^{-/-}$ TEa mice. TCR transgenic (Vα2^{+}Vβ6^{+}) CD4^{+} T cells from TEa mice (B6 background; I-A^{b}, I-E^{-}) are specific for Balb/c allopeptide I-Eα$_{52–68}$ presented by B6 APCs and bound to I-A^{b}. Male mice at 8 to 10 weeks of age were used for heart transplantation, and 10-week-old B6 female mice were subjected to EAE induction. Littermates of the same sex were randomly assigned to experimental groups. Mice were housed in a specific pathogen free facility at Houston Methodist Research Institute in Houston, Texas. All animal experiments in this study were approved by the Houston Methodist Animal Care Committee in accordance with institutional animal care and use guidelines.

METHOD DETAILS

Flow cytometry—Splenocytes, lymph node cells, graft infiltrating cells (Chen et al., 2007), CNS-infiltrating cells, and cultured T cells were stained and analyzed on the LSR II flow cytometer (Beckton Dickinson), and the resulting data was processed by using FlowJo v10 software (Tree Star, Inc.). Fluorochrome-conjugated antibodies used for flow cytometry were as follows: specific for mouse CD3 (clone 145-2C11), TCRβ (H57-597), CD4 (GK1.5), CD8a (53-6.7), CD138 (281-2), GL7 (GL7), CD25 (PC61), CD62L (MEL-14), KLRG1 (MAFA), CD44 (IM7), CD45.1 (A20), CD45.2 (104), TCR Vα2 (B20.1), TCR Vβ6 (RR4-7), PD1 (29F.1A12), CD160 (7H1), Lag3 (C9B7W), CD73 (TY/11.8), FR4 (TH6), BTLA (6A6), PD-L1 (MIH5), Tim3 (B8.2C12), CD69 (H1.2F3), GITR (DTA), 4-1BB (17B5), 2B4 (m2B4 (B6)458.1), CD226 (480.1), CTLA-4 (UC10-4B9), ICOS (C398.4A), CD98 (RL388), CD71 (RI7217), TNF-α (MP6-XT22), IL-2 (JES6-5H4), IFN-γ (XMG1.2), IL-4 (11B11), IL-10 (JES5-16E3), IL-17A (TC11-18H10.1), IL-17F (9D3.1C8), Helios (22F6), CD45 (30-F11), Perforin (eBioOMAK-D), Granzyme B (GB11), BTLA (6A6), GM-CSF (MP1-22E9), IL-13 (eBio13A), CD19 (6D5), FoxP3 (FJK-16S), Ki67 (SolA15), BCL6 (K112-91), GLUT1, (SPM498), Fluorescein labeled Peanut Agglutinin (PNA), CXCR5 (2G8), APC Streptavidin, and BV421 Streptavidin. Dead cells were excluded from some analysis by using Zombie Aqua™ Fixable Viability Kit (BioLegend). T cell proliferation was assessed by using the CellTrace™ Violet (CTV) Kit (Thermo Fisher

Scientific). Intracellular expression of GLUT1, CTLA-4, and transcription factors were determined by using the Foxp3/Transcription Factor Staining Buffer Set (eBioscience) according to the manufacturers' instructions. For intracellular staining of cytokines, cultured or *ex vivo* isolated T cells were re-stimulated for 4 hours with 50 ng/ml phorbol 12-myristate 13-acetate (Sigma-Aldrich) and 500 ng/ml ionomycin (Sigma-Aldrich) in the presence of GolgiStop (BD Biosciences). Cells were fixed and permeabilized with Cytofix/Cytoperm™ solution (BD Biosciences), followed by staining with fluorochrome-labeled antibodies against cytokines according to the manufacturers' instructions. For intracellular staining of IRF4, IRF4 antibody (M-17, goat polyclonal IgG) was purchased from Santa Cruz Biotechnology. Donkey anti-Goat IgG (H+L) Secondary Antibody conjugated with Alexa Fluor 488 or Alexa Fluor 647 was purchased from Thermo Fisher Scientific. T cells were fixed and permeabilized using the Foxp3/Transcription Factor Staining Buffer Set (eBioscience), and stained with IRF4 antibody and then with Donkey anti-Goat IgG (H+L) Secondary Antibody.

Murine heterotopic heart transplantation—Heart transplantation in mice was performed by a previously described method (Miyahara et al., 2012; Chen et al., 2007). In brief, hearts from Balb/c donors were transplanted into 8 to 10-week-old male WT B6, *Irf4*$^{fl/fl}$*Cd4-Cre*, CD45.1^{+} congenic, or *Rag1*$^{-/-}$ recipient mice. Pulmonary artery and aorta of donor heart were cut open, remaining heart vessels were tied off, and heart was removed. Anesthetized recipient mouse was opened by the midline incision and blood flow of the abdominal aorta and inferior vena cava was interrupted by ligation with 6-0 silk thread. Incisions were made in recipient abdominal aorta and inferior vena cava to perform anastomosis with donor heart aorta and donor pulmonary artery, respectively. Anastomosis was made by 11-0 sutures running continuously. 6-0 silk thread was removed and abdomen was then closed by 5-0 sutures in two layers. Heart graft survival was monitored daily by palpation, and the day of complete cessation of heartbeat was considered as the day of rejection. Recipient mice were i.p. injected with Rat IgG, anti-PD-L1 (10F.9G2), anti-CTLA-4 (9D9), anti-CD4 (GK1.5), anti-CD8 (53-6.7), or anti-CD25 (PC-61.5.3) mAbs obtained from Bio-X-Cell (West Lebanon, NH), oral gavaged with trametinib (Selleck Chemicals, Houston, TX) or corn oil, or i.v. transferred with WT B6, *Irf4*$^{-/-}$, TEa, TEa *Irf4*$^{-/-}$, or IRF4 re-introduced *Irf4*$^{-/-}$ T cells. At various days post-transplant, splenocytes and graft infiltrating cells were obtained for flow cytometry analysis, and allografts were sectioned and stained with hematoxylin and eosin for microscopic evaluation.

Reconstitution of *Rag1*$^{-/-}$ mice with T cells—In the adoptive co-transfer model, Dynabeads Untouched Mouse T Cells Kit (Thermo Fisher Scientific) was used to isolate T cells from spleens of CD45.1^{+} congenic or *Irf4*$^{-/-}$ mice. *Rag1*$^{-/-}$ mice were co-injected i.v. with 2×10^{7} CD45.1^{+} congenic WT and 2×10^{7} CD45.2^{+} (CD45.1^{-}) *Irf4*$^{-/-}$ T cells on day −1, and transplanted with Balb/c hearts on day 0. In the model transferred with separated T cell populations, 5×10^{6} FACS-sorted CD4^{+} WT, CD4^{+} *Irf4*$^{-/-}$, CD8^{+} WT, or CD8^{+} *Irf4*$^{-/-}$ T cells were injected i.v. into *B6.Rag1*$^{-/-}$ mice one day prior to BALB/c heart transplantation, respectively. Splenocytes and graft-infiltrating cells were obtained on day 9 for flow cytometry analysis.

Adoptive transfer of Tea transgenic T cells—TCR(Vα2$^+$Vβ6$^+$)CD4$^+$ TEa cells were sorted from spleens of WT TEa or *Irf4*$^{-/-}$ TEa mice by a FACSAria flow cytometer (BD Biosciences). B6.SJL CD45.1$^+$ congenic mice were i.v. transferred with either 5 × 10^6 CD45.2$^+$ WT TEa or 5 × 10^6 CD45.2$^+$ *Irf4*$^{-/-}$ TEa cells on day −1, transplanted with Balb/c hearts or left un-transplanted on day 0, followed by flow cytometry analysis of TEa cells in spleens on day 6 or 7 as indicated in text. To assess TEa cell proliferation in response to heart transplantation, WT TEa or *Irf4*$^{-/-}$ TEa cells were labeled CellTrace™ Violet prior to cell transfer. To determine effects of checkpoint blockade on *Irf4*$^{-/-}$ TEa cells, CD45.1$^+$ heart-transplanted recipients were transferred with CD45.2$^+$ *Irf4*$^{-/-}$ TEa cells and treated with either rat IgG or anti-PD-L1 plus anti-CTLA-4 mAbs. To determine effects of trametinib on WT TEa cells, CD45.1$^+$ heart-transplanted recipients were transferred with CD45.2$^+$ WT TEa cells and treated with either corn oil or trametinib.

Induction and assessment of EAE—10-week-old female B6 mice were subjected to EAE induction by using the Hooke Kit™ MOG35-55/CFA Emulsion PTX (EK-0113; Hooke Laboratories, Lawrence, MA) according to the manufacturer's instructions, and were orally gavaged with corn oil or 3 mg/kg trametinib every other day from day 0 to day 12 post immunization. Mice were monitored daily for the development of clinical signs of EAE and scored according to the previously reported criteria (Lee et al., 2012). At 18–20 days post induction of EAE, mice were euthanized for flow cytometry analysis of T cells in CNS, spleen, and draining lymph nodes of the sites of immunization. Methods for isolation of CNS-infiltrating mononuclear cells have been previously reported (Lee et al., 2012; Xiao et al., 2016).

***In vitro* T cell stimulation—**Naive CD4$^+$ T cells (CD62L$^+$CD44$^-$ or CD62L$^+$CD44$^-$FoxP3GFP$^-$) were sorted from WT B6, *Irf4*$^{-/-}$, or *Foxp3gfp* reporter mice by a FACSAria flow cytometer. B6 APCs were prepared by depletion of T cells from B6 splenocytes with phycoerythrin–anti-CD3 (clone 2C11; BioLegend) and anti-phycoerythrin microbeads (Miltenyi Biotec, San Diego, CA), followed by brief treatment with 50 μg/ml mitomycin C (Fisher Scientific) before each experiment. For activation of T cells, naïve CD4$^+$ T cells were added at 1×10^5 cells/well in 96-well round bottom tissue-culture plates (Thermo Fisher Scientific), and stimulated with equal numbers of B6 APCs and 1 μg/ml soluble anti-CD3e mAb (clone 2C11; BioLegend). For some experiments cell cultures were supplemented with various cytokines (PeproTech, Rocky Hill, NJ) and small-molecule inhibitors (Selleck Chemicals). In some cases, naïve CD4$^+$ T cells were labeled with CellTrace™ Violet reagent prior to stimulation. CD4$^+$ T cells cultured for different days were collected and analyzed with flow cytometry, microarray analysis, Immunoblot, and quantitative real-time PCR, and ChIP.

Polarization of CD4$^+$ T cells *in vitro*—For Th17 polarization, WT naïve CD4$^+$ cells were activated for 3 days in the presence of 1 ng/ml human TGF-β1, 10 ng/ml mouse IL-6, 10 ng/ml IL-1β, 10 ng/ml IL-23, 5 μg/ml anti-IL-2 (JES6-1A12), 5 μg/ml anti-IL-4 (11B11), and 5 μg/ml anti-IFN-γ (XMG 1.2), followed by flow cytometry analysis of IL-17A and IL-17F expressions. For some experiments cell cultures were supplemented with 0.2% DMSO or 100 nM trametinib. Recombinant cytokines were purchased from PeproTech and

R&D systems, and cytokine-neutralizing antibodies were purchased from BioLegend. For Th1 polarization, WT naïve $CD4^+$ cells were activated for 3 days in the presence of 10 ng/ml IL-12 (PeproTech) and 5 μg/ml anti-IL-4. Cell cultures were treated with DMSO or 100 nM trametinib. IFN-γ and IL-4 expressions were assessed by flow cytometry analysis. For iTreg polarization, $FoxP3GFP^-$ naïve $CD4^+$ T cells were activated for 3 days in the presence of 3 ng/ml TGF-β1. Cell cultures were treated with DMSO or 100 nM trametinib. FoxP3GFP expression was assessed by flow cytometry analysis.

***In vitro* suppression assay—**The responder $CD4^+$ T cells were isolated from $CD45.1^+$ congenic mice by using the Dynabeads™ Untouched™ Mouse CD4 Cells Kit (Thermo Fisher Scientific), and then labeled with CTV. Dynabeads™ FlowComp™ Mouse $CD4^+CD25^+$ Treg Cells Kit (Thermo Fisher Scientific) was used to isolate Treg cells from the spleens of naïve B6 or *Irf4*$^{fl/fl}$*Cd4-Cre* mice, or from the spleens of *Irf4*$^{fl/fl}$*Cd4-Cre* recipients at day 7 after heart transplantation (treated with either Rat IgG or anti-CTLA-4 plus anti-PD-L1 mAbs). CTV-labeled $CD45.1^+CD4^+$ T cells were added at 1×10^5 cells/well in 96-well round bottom tissue-culture plates together with or without equal numbers of Treg cells from different groups, and stimulated with T-cell–depleted mitomycin C-treated B6 splenocytes and 1 μg/ml soluble anti-CD3e mAb. Three days later, $CD45.1^+CD4^+$ T cells were analyzed for proliferation by CTV dilution using a LSR II flow cytometer.

Quantitative RT-PCR—Total RNA was extracted from activated WT and *Irf4*$^{-/-}$ $CD4^+$ T cells using a RNeasy mini kit (Qiagen), and cDNA was synthesized using the iScript™ Reverse Transcription Supermix (Bio-rad). All target primers were predesigned KiCqStart Primers (Sigma-aldrich). Transcription of target genes was calculated according to the $2^{-\Delta CT}$ method as described by the manufacturer (CFX96 Touch Real-Time PCR Detection System; Bio-rad). Gene expression results were expressed as arbitrary units relative to the expression of *Gapdh*.

Immunoblot analysis—Protein extracts were resolved by SDS-PAGE, transferred onto an Immunobilon membrane, and analyzed by immunoblot with anti-IRF4 (sc-6059; Santa Cruz), anti-BATF (8638; Cell Signaling Technology), and anti-β-actin (12262; Cell Signaling Technology). Horseradish peroxidase–linked antibody to rabbit immunoglobulin G (7074; Cell Signaling Technology), horseradish peroxidase–linked antibody to goat immunoglobulin G (sc-2768; Santa Cruz), and horseradish peroxidase–linked antibody to mouse immunoglobulin G (7076; Cell Signaling Technology) were used as secondary antibodies. Protein expression was detected by chemiluminescence.

Chromatin immunoprecipitation—Chromatin immunoprecipitation (ChIP) assays were performed as previously described (Xiao et al., 2016). All primers used in ChIP-PCR and the reported IRF4 binding site in *Ikzf2* intron (Li et al., 2012) are displayed in Figure S3. In brief, naïve WT or *Irf4*$^{-/-}$ $CD4^+$ T cells were activated *in vitro* for 48 hours and then fixed with formaldehyde. Chromatin was extracted from 1×10^6 cells for each immunoprecipitation. Anti-Histone H3K9me3 (61013; Active Motif), anti-H3K4me3 (17-678; Millipore), anti-H3Ac (39139; Active Motif), anti-H4Ac (39925; Active Motif), anti-Helios (sc-9864; Santa Cruz), anti-IRF4 (sc-6059, Santa Cruz), and isotype-matched

control antibody (sc-2027; Santa Cruz) were used for immunoprecipitation of chromatin with an EZ ChIP kit according to the manufacturer's instructions (Millipore). The precipitated DNA was then analyzed by real-time PCR. Data are presented as relative binding based on normalization to input DNA.

Retrovirus-mediated gene expression—cDNA fragments encoding mouse *Irf4* and *Ikzf2* were amplified by PCR and then cloned into a pMYs-IRES-EGFP retroviral vector (Cell Biolabs). Retroviral particles were produced by transfecting plat-E cells with those retroviral vectors according to the manufacturer's recommendations (Cell Biolabs). For T cell transduction, naïve WT or *Irf4*$^{-/-}$ CD4^{+} T cells were activated for 24 hours with B6 APCs and 1 μg/ml soluble anti-CD3 mAb, and then incubated with freshly prepared retroviral particles by centrifugation for 2 hours at 780g and 32 °C in the presence of 8 μg/ml polybrene (Sigma-Aldrich). After centrifugation, cells were first cultured for 6 hours at 32 °C, and subsequently cultured for additional 3 days in complete RPMI 1640 medium at 37 °C prior to flow cytometry analysis. For preparing IRF4 re-introduced alloreactive *Irf4*$^{-/-}$ CD4^{+} T cells, Balb/c splenic DCs were isolated by using the Pan Dendritic Cell Isolation Kit (Miltenyi Biotec). *Irf4*$^{-/-}$ CD4^{+} T cells were activated for 3 days with Balb/c splenic DCs and 100 IU IL-2, and incubated with freshly prepared retroviral particles as mentioned above. Cells were cultured for one day after transduction, and then adoptively transferred into *Irf4*$^{fl/fl}$*Cd4-Cre* mice on day 1 post-heart transplantation.

Retrovirus-mediated *Ikzf2* knockdown—The shRNA sequences for *Ikzf2* were designed by using the online tool (https://rnaidesigner.thermofisher.com). Five top listed shRNA sequences were selected and synthesized at IDT. Two complementary oligos were annealed at annealing buffer and ligated into shRNA vector (pSIREN-RetroQ-ZsGreen) from Clontech. After BamHI and EcoRI digestion, positive colonies were further verified by direct sequencing. The knockdown efficiency for each shRNA was measured in activated *Irf4*$^{-/-}$ CD4^{+} T cells by FACS, and the most potent shRNAs (Target sequence: GCAGGTCATGAGTCACCATGT) were selected for performing the following experiment: *Irf4*$^{-/-}$ CD4^{+} T cells were activated for 24 hours with B6 APCs and 1 μg/ml soluble anti-CD3 mAb, and then incubated with freshly prepared retroviral particles by centrifugation for 2 hours at 780g and 32 °C in the presence of 8 μg/ml polybrene. After centrifugation, cells were first cultured for 6 hours at 32 °C, and subsequently cultured for additional 3 days in complete RPMI 1640 medium at 37 °C prior to assessing Helios and PD-1 expressions.

Microarray and GO Enrichment Analysis—Microarray was performed by the Genomic and RNA Profiling Core at Baylor College of Medicine and data generated has been deposited in NCBI's Gene Expression Omnibus with accession number GSE83283. Naive CD4^{+} T cells (CD62L^{+}CD44^{-}) were sorted from WT B6 or *Irf4*$^{-/-}$ mice a FACSAria flow cytometer, and activated *in vitro* with soluble anti-CD3 mAb (2C11) and mitomycin C-treated APCs in 96-well round bottom tissue-culture plates. Forty-eight hours later, living CD4^{+} T cells were sorted from cultures by flow cytometry. Total RNA was extracted with RNeasy mini kit (Qiagen). RNA was quantified using a NanoDrop-1000 spectrophotometer and quality was monitored with the Agilent 2100 Bioanalyzer (Agilent Technologies). Cyanine-3 labeled cRNA was prepared from 0.5 μg RNA using the One-Color Low RNA

Input Linear Amplification PLUS kit (Agilent Technologies) and hybridized to Agilent SurePrint G3 Mouse GE v2 8×60K Microarray (G4852B; 074809). Slides were scanned immediately after washing on the Agilent Technologies Scanner (G2505C). Data were normalized and analyzed using the Subio Platform (Subio). Gene Ontology (GO) enrichment was performed using PANTHER (Annotation Version: GO Ontology database Released 2015-08-06).

QUANTIFICATION AND STATISTICAL ANALYSIS

Data were represented as mean ± SD and analyzed with Prism version 7.0a (GraphPad Software). The *P* values of EAE clinical scores and graft survival were determined by the Mann-Whitney test. Other measurements were performed using unpaired Student's *t*-test. The sample size chosen for the animal experiments was estimated based on the literature and our previous experience of performing similar sets of experiments. Differences were considered significant when $P < 0.05$. *P* values are denoted in figures as follows: n.s., $P > 0.05$; *, $P < 0.05$; and **, $P < 0.01$.

DATA AND SOFTWARE AVAILABILITY

Microarray data for this project have been deposited at NCBI's Gene Expression Omnibus (GEO) with the accession number GSE83283.

Supplementary Material

Refer to Web version on PubMed Central for supplementary material.

Acknowledgments

We thank the flow cytometry and the pathology core facilities at Houston Methodist for excellent services and Dr. Zhiqiang Zhang for discussions. We thank the Genomic and RNA Profiling Core at Baylor College of Medicine for excellent services. This study was supported by a grant from the American Heart Association (11SDG7690000 to W.C.), the startup fund from Houston Methodist Research Institute (to W.C.), and the US National Institutes of Health grant (#NIH R01AI106200 to X.C.L.).

References

Alhamad T, Venkatachalam K, Linette GP, Brennan DC. Checkpoint Inhibitors in Kidney Transplant Recipients and the Potential Risk of Rejection. Am J Transplant. 2016; 16:1332–1333. [PubMed: 26752406]

Bally AP, Austin JW, Boss JM. Genetic and Epigenetic Regulation of PD-1 Expression. J Immunol. 2016; 196:2431–2437. [PubMed: 26945088]

Baumeister SH, Freeman GJ, Dranoff G, Sharpe AH. Coinhibitory Pathways in Immunotherapy for Cancer. Annu Rev Immunol. 2016; 34:539–573. [PubMed: 26927206]

Bollig N, Brustle A, Kellner K, Ackermann W, Abass E, Raifer H, Camara B, Brendel C, Giel G, Bothur E, et al. Transcription factor IRF4 determines germinal center formation through follicular T-helper cell differentiation. Proc Natl Acad Sci USA. 2012; 109:8664–8669. [PubMed: 22552227]

Bolton EM, Gracie JA, Briggs JD, Kampinga J, Bradley JA. Cellular requirements for renal allograft rejection in the athymic nude rat. J Exp Med. 1989; 169:1931–1946. [PubMed: 2659723]

Brustle A, Heink S, Huber M, Rosenplanter C, Stadelmann C, Yu P, Arpaia E, Mak TW, Kamradt T, Lohoff M. The development of inflammatory T(H)-17 cells requires interferon-regulatory factor 4. Nat Immunol. 2007; 8:958–966. [PubMed: 17676043]

Chen W, Diao J, Stepkowski SM, Zhang L. Both infiltrating regulatory T cells and insufficient antigen presentation are involved in long-term cardiac xenograft survival. J Immunol. 2007; 179:1542–1548. [PubMed: 17641020]

Conlon TM, Saeb-Parsy K, Cole JL, Motallebzadeh R, Qureshi MS, Rehakova S, Negus MC, Callaghan CJ, Bolton EM, Bradley JA, et al. Germinal center alloantibody responses are mediated exclusively by indirect-pathway CD4 T follicular helper cells. J Immunol. 2012; 188:2643–2652. [PubMed: 22323543]

Crawford A, Angelosanto JM, Kao C, Doering TA, Odorizzi PM, Barnett BE, Wherry EJ. Molecular and transcriptional basis of CD4(+) T cell dysfunction during chronic infection. Immunity. 2014; 40:289–302. [PubMed: 24530057]

Cretney E, Xin A, Shi W, Minnich M, Masson F, Miasari M, Belz GT, Smyth GK, Busslinger M, Nutt SL, et al. The transcription factors Blimp-1 and IRF4 jointly control the differentiation and function of effector regulatory T cells. Nat Immunol. 2011; 12:304–311. [PubMed: 21378976]

Fathman CG, Lineberry NB. Molecular mechanisms of CD4+ T-cell anergy. Nat Rev Immunol. 2007; 7:599–609. [PubMed: 17612584]

Grumont RJ, Gerondakis S. Rel induces interferon regulatory factor 4 (IRF-4) expression in lymphocytes: modulation of interferon-regulated gene expression by rel/nuclear factor kappaB. J Exp Med. 2000; 191:1281–1292. [PubMed: 10770796]

Grusdat M, McIlwain DR, Xu HC, Pozdeev VI, Knievel J, Crome SQ, Robert-Tissot C, Dress RJ, Pandyra AA, Speiser DE, et al. IRF4 and BATF are critical for CD8(+) T-cell function following infection with LCMV. Cell Death Differ. 2014; 21:1050–1060. [PubMed: 24531538]

Gupta S, Balasubramanian S, Thornley TB, Strom TB, Kenny JJ. Direct pathway T-cell alloactivation is more rapid than indirect pathway alloactivation. Transplantation. 2011; 91:e65–67. [PubMed: 21508799]

Huber M, Brustle A, Reinhard K, Guralnik A, Walter G, Mahiny A, von Löw E, Lohoff M. IRF4 is essential for IL-21-mediated induction, amplification, and stabilization of the Th17 phenotype. Proc Natl Acad Sci USA. 2008; 105:20846–20851. [PubMed: 19088203]

Huber M, Lohoff M. IRF4 at the crossroads of effector T-cell fate decision. Eur J Immunol. 2014; 44:1886–1895. [PubMed: 24782159]

Kim HJ, Barnitz RA, Kreslavsky T, Brown FD, Moffett H, Lemieux ME, Kaygusuz Y, Meissner T, Holderried TA, Chan S, et al. Stable inhibitory activity of regulatory T cells requires the transcription factor Helios. Science. 2015; 350:334–339. [PubMed: 26472910]

Krieger NR, Yin DP, Fathman CG. CD4+ but not CD8+ cells are essential for allorejection. J Exp Med. 1996; 184:2013–2018. [PubMed: 8920888]

Larkin J, Chiarion-Sileni V, Gonzalez R, Grob JJ, Cowey CL, Lao CD, Schadendorf D, Dummer R, Smylie M, Rutkowski P, et al. Combined Nivolumab and Ipilimumab or Monotherapy in Untreated Melanoma. N Engl J Med. 2015; 373:23–34. [PubMed: 26027431]

Lechler RI, Sykes M, Thomson AW, Turka LA. Organ transplantation–how much of the promise has been realized? Nat Med. 2005; 11:605–613. [PubMed: 15937473]

Lee Y, Awasthi A, Yosef N, Quintana FJ, Xiao S, Peters A, Wu C, Kleinewietfeld M, Kunder S, Hafler DA, et al. Induction and molecular signature of pathogenic TH17 cells. Nat Immunol. 2012; 13:991–999. [PubMed: 22961052]

Li P, Spolski R, Liao W, Wang L, Murphy TL, Murphy KM, Leonard WJ. BATF-JUN is critical for IRF4-mediated transcription in T cells. Nature. 2012; 490:543–546. [PubMed: 22992523]

Lipson EJ, Bagnasco SM, Moore J Jr, Jang S, Patel MJ, Zachary AA, Pardoll DM, Taube JM, Drake CG. Tumor Regression and Allograft Rejection after Administration of Anti-PD-1. N Engl J Med. 2016; 374:896–898.

Liu Z, Fan H, Jiang S. CD4(+) T-cell subsets in transplantation. Immunol Rev. 2013; 252:183–191. [PubMed: 23405905]

Mahnke J, Schumacher V, Ahrens S, Kading N, Feldhoff LM, Huber M, Rupp J, Raczkowski F, Mittrucker HW. Interferon Regulatory Factor 4 controls TH1 cell effector function and metabolism. Sci Rep. 2016; 6:35521. [PubMed: 27762344]

Man K, Miasari M, Shi W, Xin A, Henstridge DC, Preston S, Pellegrini M, Belz GT, Smyth GK, Febbraio MA, et al. The transcription factor IRF4 is essential for TCR affinity-mediated metabolic

programming and clonal expansion of T cells. Nat Immunol. 2013; 14:1155–1165. [PubMed: 24056747]

Martinez RJ, Zhang N, Thomas SR, Nandiwada SL, Jenkins MK, Binstadt BA, Mueller DL. Arthritogenic self-reactive CD4+ T cells acquire an FR4hiCD73hi anergic state in the presence of Foxp3+ regulatory T cells. J Immunol. 2012; 188:170–181. [PubMed: 22124124]

Mittrucker HW, Matsuyama T, Grossman A, Kundig TM, Potter J, Shahinian A, Wakeham A, Patterson B, Ohashi PS, Mak TW. Requirement for the transcription factor LSIRF/IRF4 for mature B and T lymphocyte function. Science. 1997; 275:540–543. [PubMed: 8999800]

Miyahara Y, Khattar M, Schroder PM, Mierzejewska B, Deng R, Han R, Hancock WW, Chen W, Stepkowski SM. Anti-TCRbeta mAb induces long-term allograft survival by reducing antigen-reactive T cells and sparing regulatory T cells. Am J Transplant. 2012; 12:1409–1418. [PubMed: 22420295]

Murphy TL, Tussiwand R, Murphy KM. Specificity through cooperation: BATF-IRF interactions control immune-regulatory networks. Nat Rev Immunol. 2013; 13:499–509. [PubMed: 23787991]

Nayar R, Enos M, Prince A, Shin H, Hemmers S, Jiang JK, Klein U, Thomas CJ, Berg LJ. TCR signaling via Tec kinase ITK and interferon regulatory factor 4 (IRF4) regulates CD8+ T-cell differentiation. Proc Natl Acad Sci USA. 2012; 109:E2794–2802. [PubMed: 23011795]

Notarangelo LD. Functional T cell immunodeficiencies (with T cells present). Annu Rev Immunol. 2013; 31:195–225. [PubMed: 23298211]

Ochiai K, Maienschein-Cline M, Simonetti G, Chen J, Rosenthal R, Brink R, Chong AS, Klein U, Dinner AR, Singh H, et al. Transcriptional regulation of germinal center B and plasma cell fates by dynamical control of IRF4. Immunity. 2013; 38:918–929. [PubMed: 23684984]

Postow MA, Chesney J, Pavlick AC, Robert C, Grossmann K, McDermott D, Linette GP, Meyer N, Giguere JK, Agarwala SS, et al. Nivolumab and ipilimumab versus ipilimumab in untreated melanoma. N Engl J Med. 2015; 372:2006–2017. [PubMed: 25891304]

Rangachari M, Kuchroo VK. Using EAE to better understand principles of immune function and autoimmune pathology. J Autoimmun. 2013; 45:31–39. [PubMed: 23849779]

Rogers NJ, Lechler RI. Allorecognition. Am J Transplant. 2001; 1:97–102. [PubMed: 12099369]

Ross EM, Bourges D, Hogan TV, Gleeson PA, van Driel IR. Helios defines T cells being driven to tolerance in the periphery and thymus. Eur J Immunol. 2014; 44:2048–2058. [PubMed: 24740292]

Safinia N, Scotta C, Vaikunthanathan T, Lechler RI, Lombardi G. Regulatory T Cells: Serious Contenders in the Promise for Immunological Tolerance in Transplantation. Front Immunol. 2015; 6:438. [PubMed: 26379673]

Schietinger A, Greenberg PD. Tolerance and exhaustion: defining mechanisms of T cell dysfunction. Trends Immunol. 2014; 35:51–60. [PubMed: 24210163]

Schietinger A, Philip M, Krisnawan VE, Chiu EY, Delrow JJ, Basom RS, Lauer P, Brockstedt DG, Knoblaugh SE, Hämmerling GJ, et al. Tumor-Specific T Cell Dysfunction Is a Dynamic Antigen-Driven Differentiation Program Initiated Early during Tumorigenesis. Immunity. 2016; 45:389–401. [PubMed: 27521269]

Singer M, Wang C, Cong L, Marjanovic ND, Kowalczyk MS, Zhang H, Nyman J, Sakuishi K, Kurtulus S, Gennert D, et al. A Distinct Gene Module for Dysfunction Uncoupled from Activation in Tumor-Infiltrating T Cells. Cell. 2016; 166:1500–1511. [PubMed: 27610572]

Staudt V, Bothur E, Klein M, Lingnau K, Reuter S, Grebe N, Gerlitzki B, Hoffmann M, Ulges A, Taube C, et al. Interferon-regulatory factor 4 is essential for the developmental program of T helper 9 cells. Immunity. 2010; 33:192–202. [PubMed: 20674401]

Vander Lugt B, Khan AA, Hackney JA, Agrawal S, Lesch J, Zhou M, Lee WP, Park S, Xu M, DeVoss J, et al. Transcriptional programming of dendritic cells for enhanced MHC class II antigen presentation. Nat Immunol. 2014; 15:161–167. [PubMed: 24362890]

Wherry EJ, Kurachi M. Molecular and cellular insights into T cell exhaustion. Nat Rev Immunol. 2015; 15:486–499. [PubMed: 26205583]

Xiao X, Shi X, Fan Y, Wu C, Zhang X, Minze L, Liu W, Ghobrial RM, Lan P, Li XC. The Costimulatory Receptor OX40 Inhibits Interleukin-17 Expression through Activation of Repressive Chromatin Remodeling Pathways. Immunity. 2016; 44:1271–1283. [PubMed: 27317259]

Yang H, Thomas D, Boffa DJ, Ding R, Li B, Muthukumar T, Sharma VK, Lagman M, Luo GX, Kapur S, et al. Enforced c-REL deficiency prolongs survival of islet allografts1. Transplantation. 2002; 74:291–298. [PubMed: 12177605]

Yao S, Buzo BF, Pham D, Jiang L, Taparowsky EJ, Kaplan MH, Sun J. Interferon regulatory factor 4 sustains CD8(+) T cell expansion and effector differentiation. Immunity. 2013; 39:833–845. [PubMed: 24211184]

Yuan X, Paez-Cortez J, Schmitt-Knosalla I, D'Addio F, Mfarrej B, Donnarumma M, Habicht A, Clarkson MR, Iacomini J, Glimcher LH, et al. A novel role of CD4 Th17 cells in mediating cardiac allograft rejection and vasculopathy. J Exp Med. 2008; 205:3133–3144. [PubMed: 19047438]

Zarour HM. Reversing T-cell Dysfunction and Exhaustion in Cancer. Clin Cancer Res. 2016; 22:1856–1864. [PubMed: 27084739]

Zheng Y, Chaudhry A, Kas A, deRoos P, Kim JM, Chu TT, Corcoran L, Treuting P, Klein U, Rudensky AY. Regulatory T-cell suppressor program co-opts transcription factor IRF4 to control T(H)2 responses. Nature. 2009; 458:351–356. [PubMed: 19182775]

Highlights

- Ablation of IRF4 induces transplant acceptance by establishing T cell dysfunction
- IRF4 represses PD-1, Helios, and other molecules associated with T cell dysfunction
- *Irf4*$^{-/-}$ T cell dysfunction is initially reversible but later becomes irreversible
- Trametinib inhibits IRF4, abrogates EAE development and prolongs allograft survival

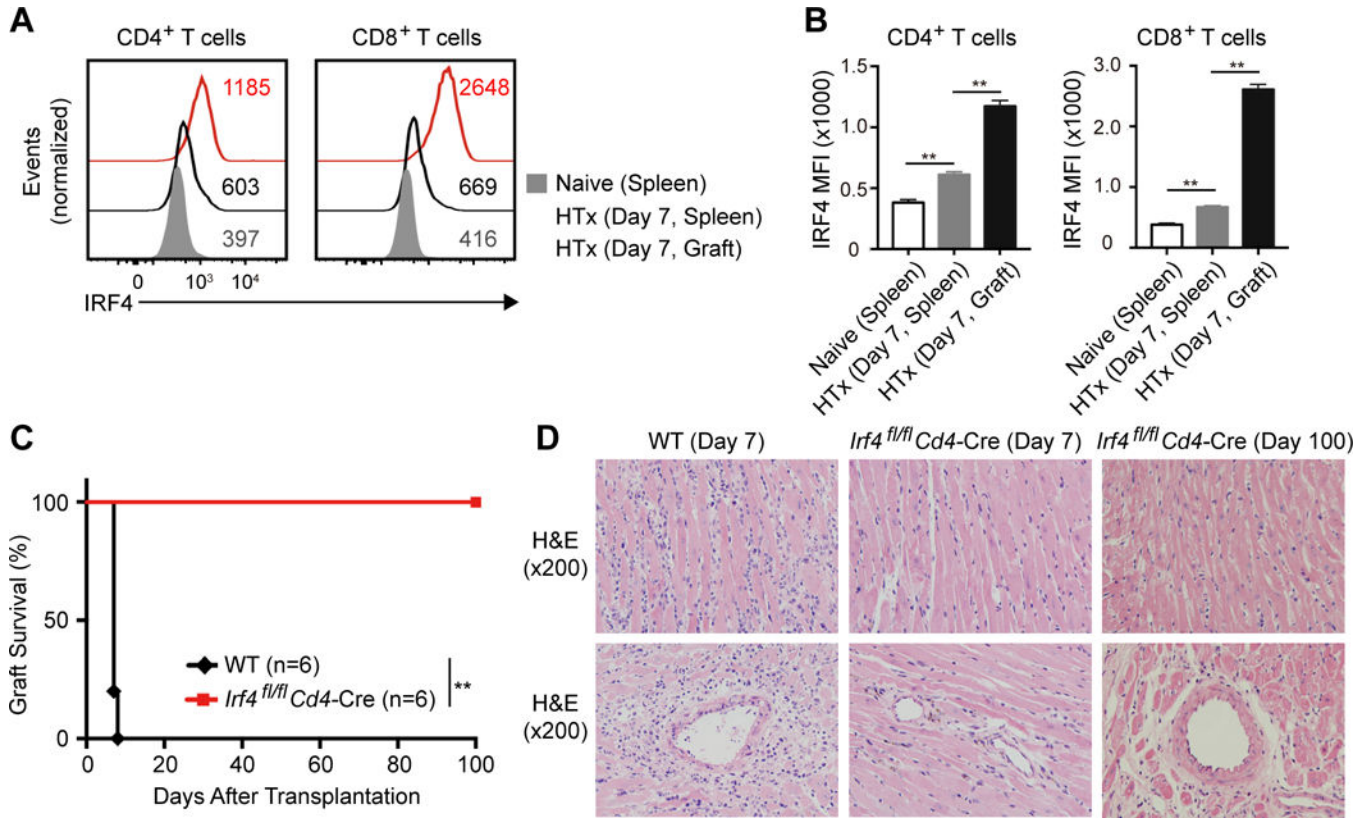

Figure 1. IRF4 is overexpressed in graft-infiltrating T cells, and *Irf4*-deficient T cells do not mediate heart allograft rejection

(A and B) Flow cytometry analysis of IRF4 expression in $CD4^+$ (left) and $CD8^+$ (right) T cells from the spleens and allografts of WT B6 recipient mice at 7 days after Balb/c heart transplantation (HTx). $CD4^+$ and $CD8^+$ T cells from the spleens of naïve B6 mice were used as controls. Representative histograms (A) and IRF4 MFI values (B) were shown. Data in (B) are presented as mean ± SD (n = 4). $^{**}P<0.01$; unpaired Student's *t*-test. Data are representative of two independent experiments. (C and D) WT B6 and $Irf4^{fl/fl}Cd4\text{-}Cre$ mice were transplanted with Balb/c hearts. (C) The percentage of allograft survival after transplantation (n=6). $^{**}P<0.01$; Mann-Whitney test. (D) H&E stained sections of heart allografts harvested from WT B6 recipients at day 7 post-transplant, or from $Irf4^{fl/fl}Cd4\text{-}Cre$ recipients at day 7 or day 100 post-transplant. Three mice per group were analyzed, with ten graft sections per mouse. Two representative images (top and bottom) per group are shown. See also Figure S1.

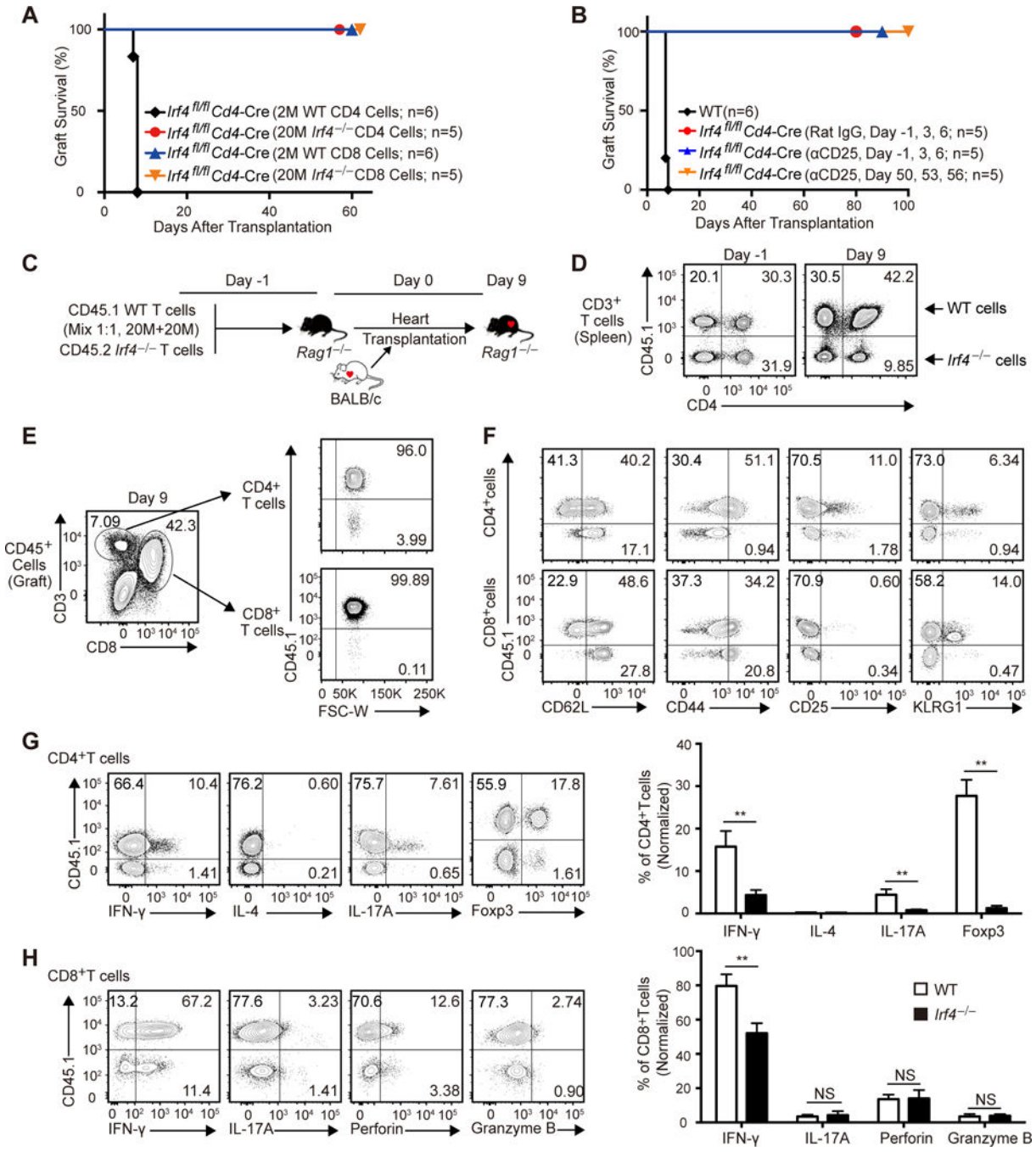

Figure 2. The dysfunction of *Irf4*-deficent T cells in transplantation is correlated with impaired cytokine production and graft infiltration

(A) Balb/c heart allograft survival in *Irf4*$^{fl/fl}$*Cd4-Cre* mice that were adoptively transferred with 2 or 20 million (M) indicated T cells. (B) Balb/c heart allograft survival in *Irf4*$^{fl/fl}$*Cd4-Cre* mice that were treated with rat IgG or an anti-CD25 (αCD25) mAb on indicated days. (C-H) *Rag1*$^{-/-}$ mice were co-injected with 2 × 10^7 (20M) CD45.1$^+$ WT and 20M CD45.2$^+$ (CD45.1$^-$) *Irf4*$^{-/-}$ T cells on day −1, and received Balb/c heart allografts on day 0. Splenocytes and graft-infiltrating cells were isolated on day 9 for flow cytometry analysis. (C) Schematic of the experimental design. (D) Representative contour plots showing %

transferred CD45.1$^+$ WT and CD45.1$^-$ *Irf4*$^{-/-}$ T cells (CD4$^+$ or CD4$^-$, gated on CD3$^+$ cells) in spleens on day −1 (left) and day 9 (right). (E) The left plot displays % CD4$^+$ (CD3$^+$CD8$^-$) and CD8$^+$ (CD3$^+$CD8$^+$) T cells among CD45$^+$ graft-infiltrating cells on day 9, and the right plots display % CD45.1$^+$ WT and CD45.1$^-$ *Irf4*$^{-/-}$ cell populations among those CD4$^+$ and CD8$^+$ infiltrating T cells. (F) Expression of indicated markers on CD4$^+$ (top) and CD8$^+$ (bottom) populations of transferred CD45.1$^+$ WT and CD45.1$^-$ *Irf4*$^{-/-}$ T cells in spleens on day 9. (G and H) Plots (left) and the bar graphs (right) depict the percentage expression of indicated molecules in co-transferred CD45.1$^+$ WT and CD45.1$^-$ *Irf4*$^{-/-}$ CD4$^+$ (G) or CD8$^+$ (H) T cells in spleens on day 9. Data are mean ± SD. $^{**}P<0.01$; unpaired student's *t*-test. Data are representative of three independent experiments with three to four mice in each group (C-H). See also Figure S2.

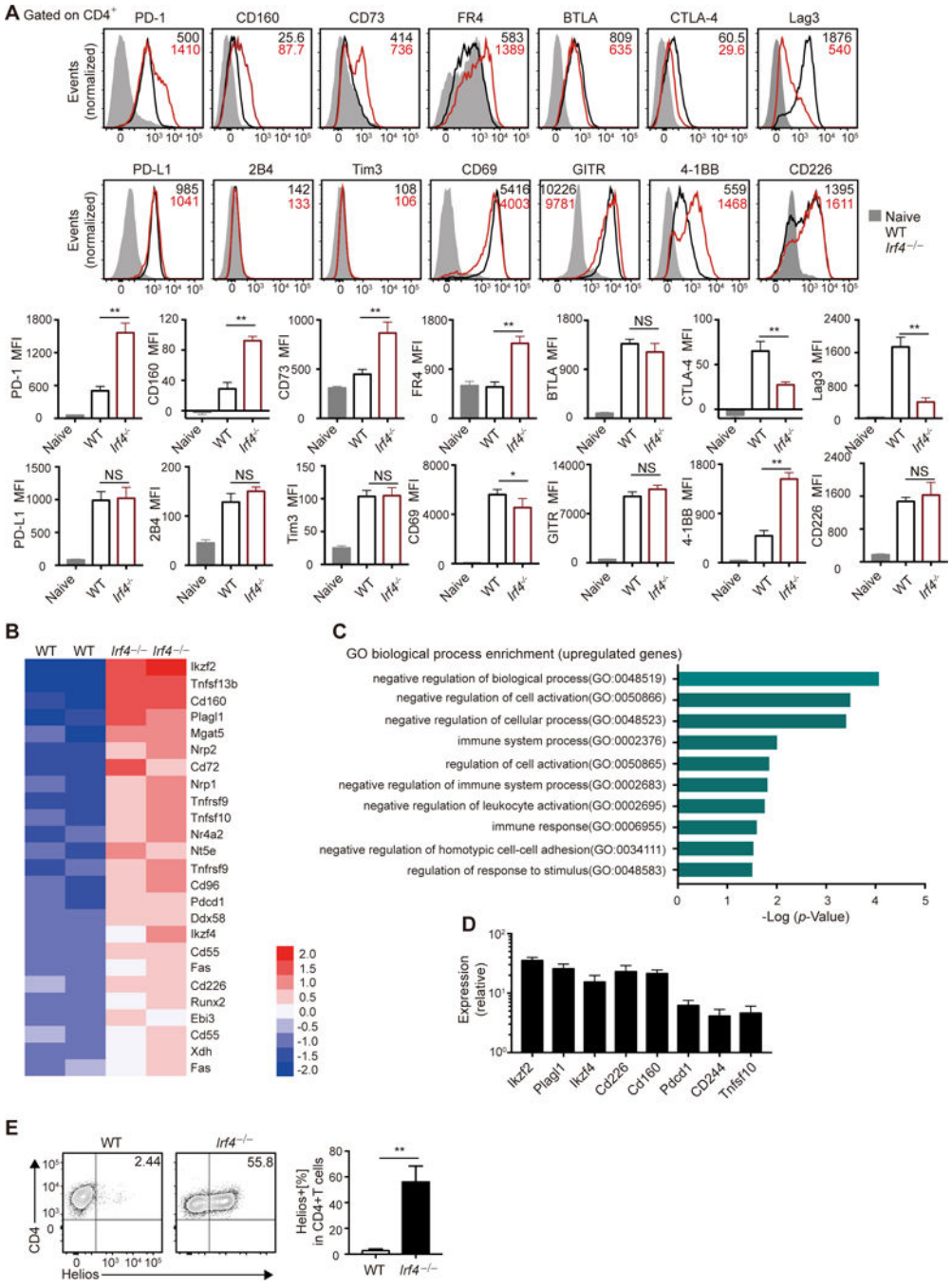

Figure 3. IRF4 represses a set of molecules associated with CD4$^+$ T cell dysfunction

(A) Flow cytometry analysis of cell surface molecules expressed on naïve WT CD4$^+$ T cells (gray shades), or on activated WT (black lines) or *Irf4*$^{-/-}$ (red lines) CD4$^+$ T cells one day after stimulation with B6 APCs (mitomycin C-treated, T-cell–depleted B6 splenocytes) and soluble anti-CD3 mAb. (B-E) WT and *Irf4*$^{-/-}$ CD4$^+$ T cells were activated for 2 days. RNA was analyzed by microarray and quantitative real-time PCR, and Helios expression was analyzed by flow cytometry. (B) Heat map showing the normalized expression scores (relative to row mean) of selected genes from WT or *Irf4*$^{-/-}$ CD4$^+$ T cells. Two RNA

samples of each group were obtained from two independent culture experiments of pooled T cells from n = 3 mice per sample. (C) GO categories enrichment analysis of 438 upregulated genes in *Irf4*$^{-/-}$ CD4^{+} T cells in accordance with biological process. The horizontal axis shows −log10 of the P-value. (D) Relative changes of mRNA expression of the indicated genes in *Irf4*$^{-/-}$ CD4^{+} T cells compared to WT CD4^{+} T cells determined by quantitative real-time PCR. Data are mean ± SD. (E) Flow cytometry analysis of Helios expression in WT and *Irf4*$^{-/-}$ CD4^{+} T cells. Data are representative of three experiments with triplicate samples (A, D, E).

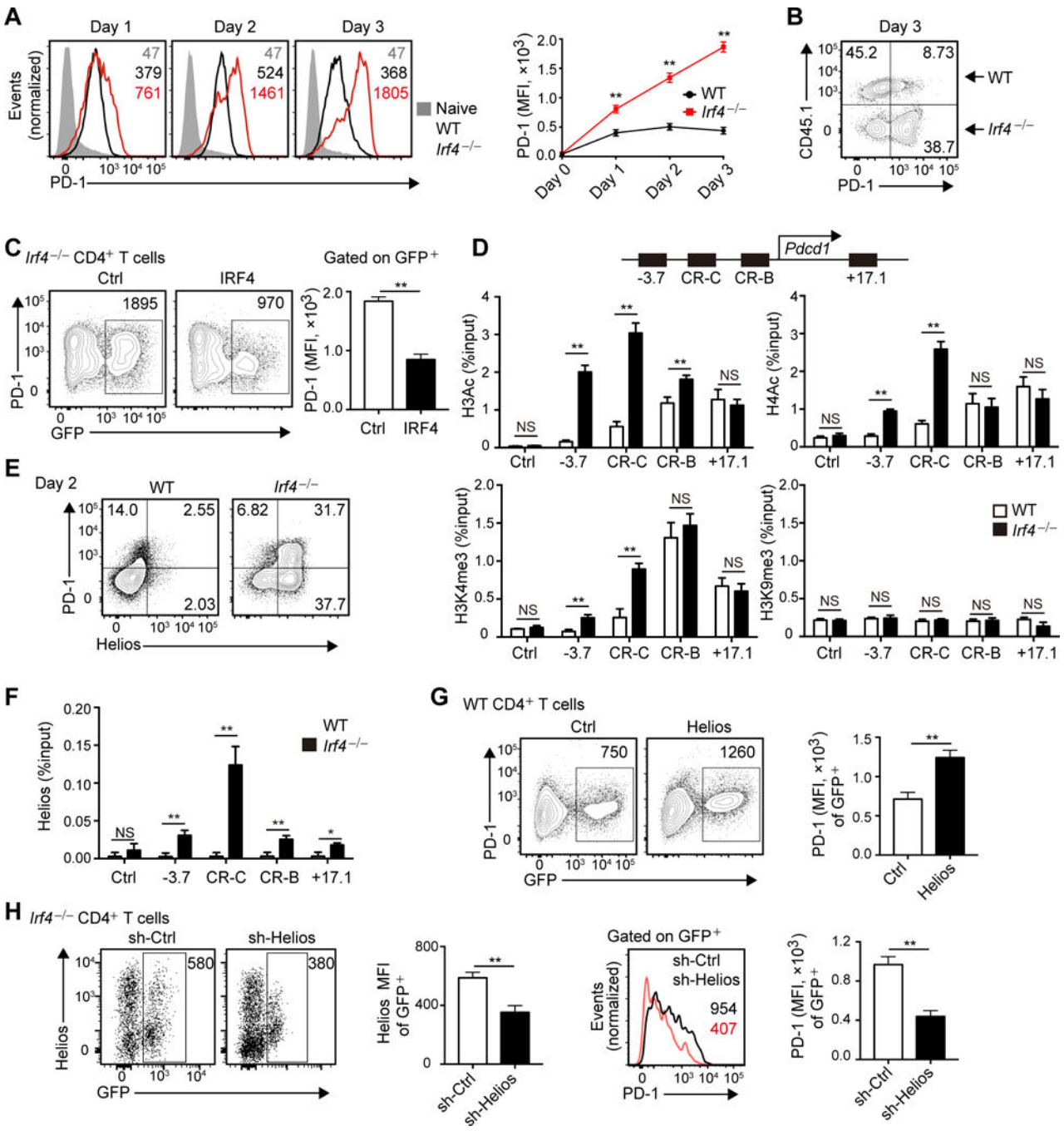

Figure 4. Upregulation of PD-1 in activated *Irf4*$^{-/-}$ CD4^{+} T cells through increased chromatin accessibility and Helios binding at PD-1 *cis*-regulatory elements

(A) Histograms show PD-1 expression (shades and lines) and MFI (numbers) on freshly isolated naïve WT CD4^{+} T cells (gray), or on activated WT (black) or *Irf4*$^{-/-}$ (red) CD4^{+} T cells at indicated days after stimulation with B6 APCs and soluble anti-CD3 mAb. Line graph (right) displays change in PD-1 MFI with time after activation. (B) PD-1 expression on co-cultured CD45.1^{+} WT and CD45.1^{-} *Irf4*$^{-/-}$ CD4^{+} T cells 3 days after activation. (C) PD-1 expression on activated *Irf4*$^{-/-}$ CD4^{+} T cells transduced with a retroviral vector expressing GFP alone (Ctrl) or with retrovirus expressing *Irf4*-GFP (IRF4). Numbers in

contour plots (left) and the bar graph (right) indicate PD-1 MFI of gated GFP^+ cells. (D) ChIP analysis of H3Ac, H4Ac, H3K4me3, and H3K9me3 at the PD-1 *cis*-regulatory elements (−3.7, *CR-C*, *CR-B*, and +17.1) in WT and $Irf4^{-/-}$ $CD4^+$ T cells 2 days after activation. (E) PD-1 and Helios expressions on WT and $Irf4^{-/-}$ $CD4^+$ T cells at 2 days after activation. (F) ChIP analysis of the enrichment of Helios at the PD-1 *cis*-regulatory elements in WT and $Irf4^{-/-}$ $CD4^+$ T cells at 2 days after activation. (G) PD-1 expression on activated WT $CD4^+$ T cells transduced with a retroviral vector expressing GFP alone (Ctrl) or with retrovirus expressing *Ikzf2*-GFP (Helios). Numbers in contour plots (left) and the bar graph (right) indicate PD-1 MFI of gated GFP^+ cells. (H) Helios (left three panels) and PD-1 (right two panels) expression by GFP^+ $Irf4^{-/-}$ $CD4^+$ T cells that were transduced with a retroviral vector co-expressing GFP and shRNA sequences for Helios (sh-Helios) or containing GFP alone (sh-Ctrl). Numbers in plots and the bar graphs indicate Helios and PD-1 MFI of gated GFP^+ cells. $*P<0.05$ and $**P<0.01$ (unpaired student's *t*-test). Data are representative of three independent experiments. See also Figure S3.

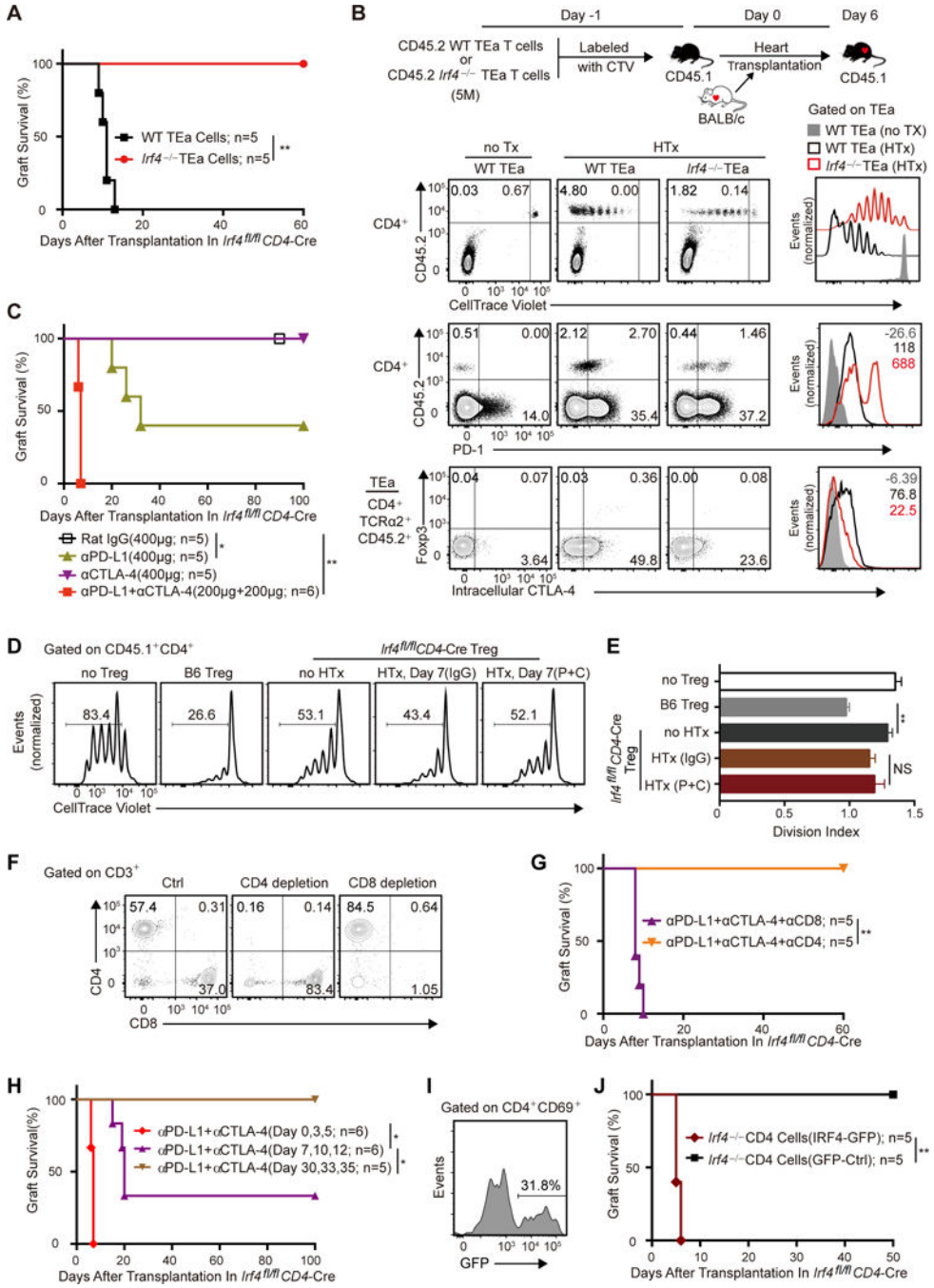

Figure 5. Responsiveness to checkpoint blockade defines the dysfunctional states of *Irf4*-deficient T cells after transplantation

(A) Balb/c heart graft survival in *Irf4*$^{fl/fl}$*Cd4-Cre* mice that were adoptively transferred with 2×10^7 WT or *Irf4*$^{-/-}$ TEa cells on day −1. (B) CD45.1$^+$ congenic mice were transferred with 5×10^6 (5M) CellTrace Violet (CTV)-labeled CD45.2$^+$ WT or *Irf4*$^{-/-}$ TEa cells on day −1, received Balb/c heart transplants (HTx) or left un-transplanted (no Tx) on day 0, followed by analysis of splenocytes on day 6. Contour plots show co-expression of CD45.2 with CTV or PD-1, gated on CD4$^+$ cells; or show co-expression of Foxp3 with intracellular CTLA-4, gated on CD4$^+$CD45.2$^+$ TCRα2$^+$ TEa cells. Histograms display CTV, PD-1, and

intracellular CTLA-4 expressions, gated on TEa cells. Data are representative of three experiments. (C) Balb/c heart graft survival in *Irf4*$^{fl/fl}$*Cd4-Cre* mice that were treated with rat IgG, anti-PD-L1, anti-CTLA-4, or anti-PD-L1 plus anti-CTLA-4 mAbs on days 0, 3, and 5 post-transplant. (D and E) Dilution of CTV (D) indicates proliferation of CD45.1$^+$ CD4$^+$ T cells in the absence or presence of Treg cells from indicated groups. Quantification of the results (E) is presented as division index. (F and G) *Irf4*$^{fl/fl}$*Cd4-Cre* mice were transplanted with Balb/c hearts and treated with anti-PD-L1 plus anti-CTLA-4 mAbs, together with 400 μg anti-CD4 or anti-CD8 depleting mAb on days 0, 3, and 5. Counter plots (F) show efficacy of T cell depletion on day 4. The graph (G) shows heart graft survival. (H) Balb/c heart graft survival in *Irf4*$^{fl/fl}$*Cd4-Cre* mice that were treated with anti-PD-L1 plus anti-CTLA-4 mAbs starting from day 0 (on days 0, 3, and 5), day 7 (on days 7, 10, and 12), or day 30 (on days 30, 33, and 35) post-transplant. (I and J) Histogram (I) shows % GFP$^+$ cells in CD4$^+$CD69$^+$ *Irf4*$^{-/-}$ cells following 3-day stimulation with Balb/c splenic DCs and 1-day IRF4-GFP viral transduction. The graph (J) shows Balb/c heart graft survival in *Irf4*$^{fl/fl}$*Cd4-Cre* mice that were transferred on day 1 with 1 × 10^6 GFP$^+$ *Irf4*$^{-/-}$ CD4 T cells (transduced with IRF4-GFP or GFP-Ctrl). $P<0.05$ and $^{**}P<0.01$; Mann-Whitney test (A, C, G, H and J). See also Figure S4.

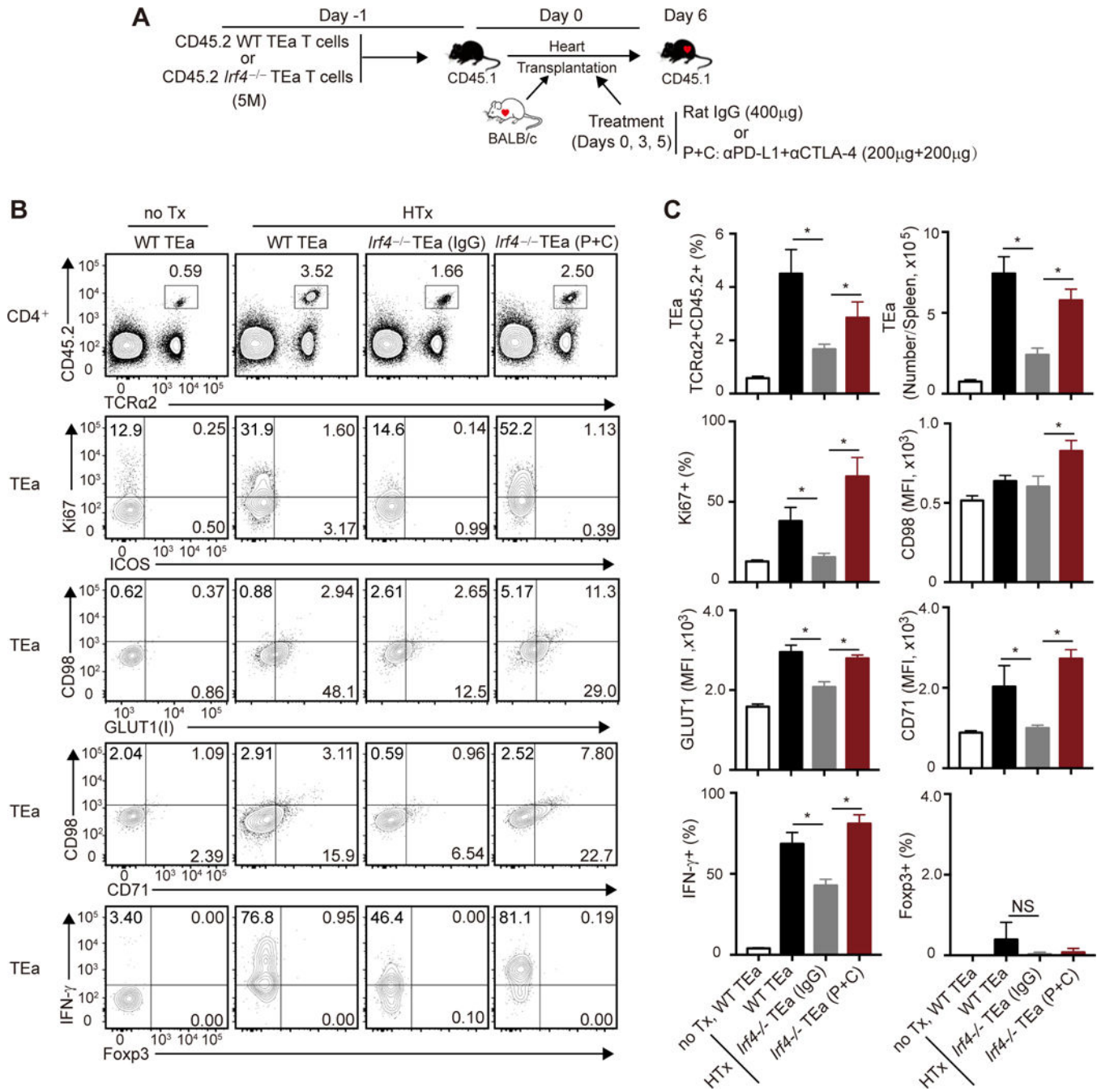

Figure 6. Checkpoint blockade reverses the initial dysfunction of *Irf4*-deficient CD4$^+$ T cells by restoring their ability to undergo proliferation and secrete IFN-γ

(A) As shown in the schematic, CD45.1$^+$ congenic mice were transferred with 5 × 10^6 (5M) CD45.2$^+$ WT or *Irf4*$^{-/-}$ TEa cells on day −1, received Balb/c heart transplants (HTx) or left un-transplanted (no Tx) on day 0, treated with rat IgG (*Irf4*$^{-/-}$ TEa (IgG)) or anti-PD-L1 plus anti-CTLA-4 mAbs (*Irf4*$^{-/-}$ TEa (P+C)) on days 0, 3, and 5, followed by flow cytometry analysis of TEa cells in spleens on day 6. (B) % transferred TEa cells among CD4$^+$ splenocytes (top row) and expression of indicated molecules by TEa splenocytes (other rows) on day 6 post-transplant. (C) Bar graphs show % TEa cells among CD4$^+$

splenocytes and numbers of TEa splenocytes (top row), and % Ki67^{+}, CD98 MFI, GLUT1 MFI, CD71 MFI, % IFN-γ^{+}, and % Foxp3^{+} of TEa cells (other rows). *P<0.05 (unpaired student's t-test). Data are mean ± SD (C) and are representative of three experiments (B and C). See also Figure S5.

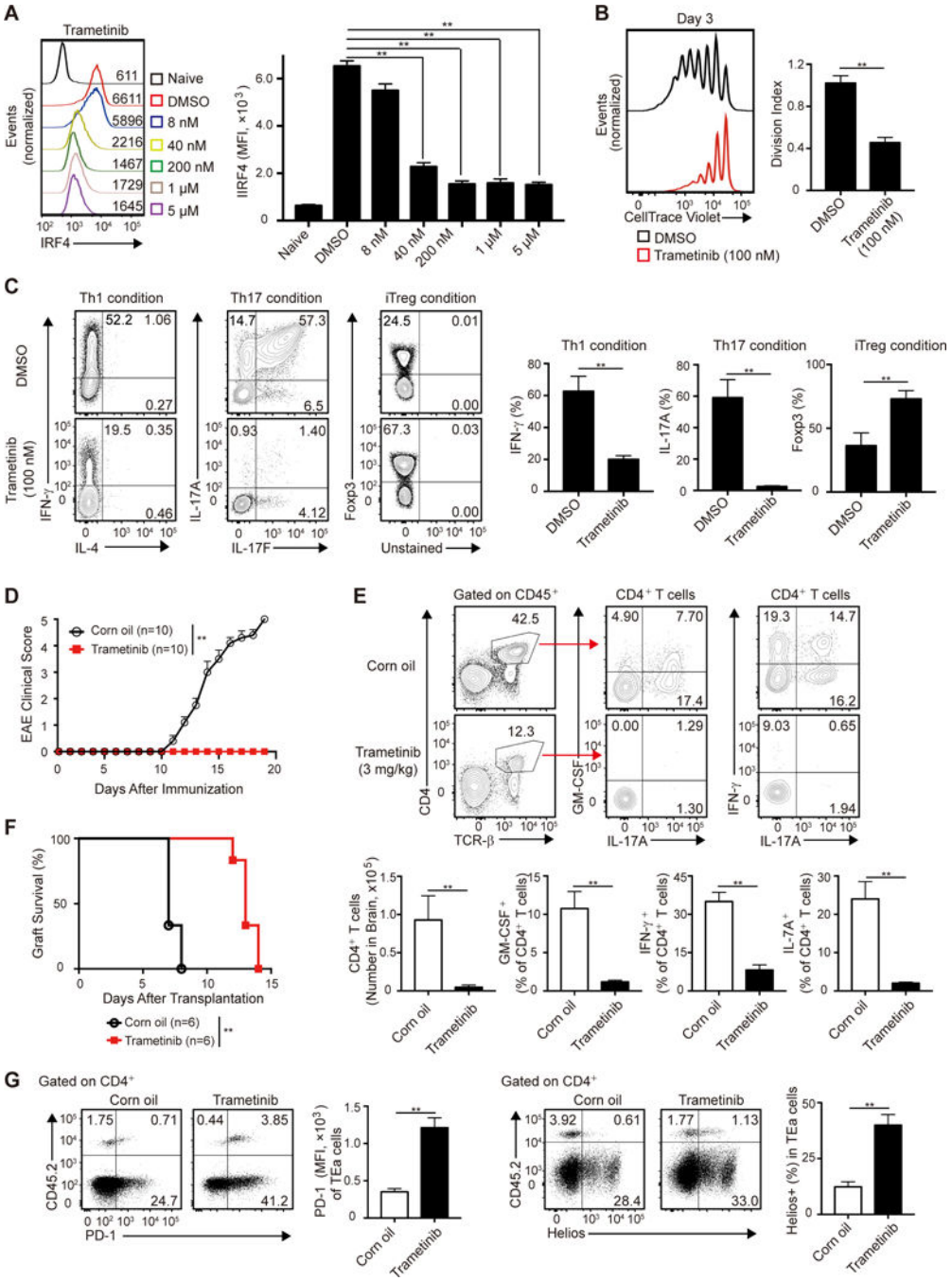

Figure 7. Trametinib inhibits IRF4 expression in T cells, prevents EAE development, and prolongs allograft survival

(A) IRF4 expression (left) and MFI (right) in freshly isolated naïve B6 CD4$^+$ T cells, or in CD4$^+$ T cells that were activated for 2 days in the presence of DMSO vehicle or varying concentrations of trametinib. (B) Dilution of CTV (left) indicates proliferation of CD4$^+$ T cells that were activated for 3 days in the presence of DMSO or 100 nM trametinib. Quantification of the results (right) is presented as division index. (C) Contour plots (left) and bar graphs (right) display frequencies of IFN-γ, IL-17, and Foxp3 expressing cells in CD4$^+$ T cells that were cultured under Th1, Th17, and inducible Treg (iTreg) polarizing

conditions for 3 days in the presence of DMSO or 100 nM trametinib. (D and E) 10-week-old B6 female mice subjected to MOG35-55–induced EAE were treated with corn oil or 3 mg/kg Trametinib every other day from day 0 to day 12 post immunization. (D) Clinical scores of mice in each group. (E) Contour plots (6 panels on the top) display the frequency of $CD4^+TCR\beta^+$ T cells among $CD45^+$ cells in the brain tissues at 18–20 days post induction of EAE, and expression of GM-CSF, IL-17A, IFN-γ by those $CD4^+$ T cells. Bar graphs (4 panels on the bottom) indicate the number of $CD4^+$ T cells in the brain tissues, and frequencies of IFN-γ^+, IL-$17A^+$, GM-CSF^+ cells among them. (F) Percentage Balb/c heart allograft survival in B6 recipients that were treated with Trametinib or corn oil every other day from day 0 to day 12 post-transplant. (G) $CD45.1^+$ mice were transferred with 5×10^6 $CD45.2^+$ WT TEa cells on day −1, received Balb/c heart transplants on day 0 and treated with corn oil or 3 mg/kg Trametinib on days 0, 2, 4, and 6, followed by analysis of splenocytes on day 7. Dot plots show co-expression of CD45.2 with PD-1 (left) or Helios (right), gated on $CD4^+$ cells. Bar graphs display PD-1 MFI and % $Helios^+$ cells of transferred $CD45.2^+$ TEa cells. Data are mean ± SD (A-C, E, and G) and are representative of two to three independent experiments. $^{**}P<0.01$; unpaired student's t-test (A-C, E, and G); Mann-Whitney test (D and F). See also Figures S6 and S7.